Dynamics amidst folding and twisting in 2-dimensional maps

Garst, Swier Harm Pieter

ISBN (Book version): 978-94-034-0945-0
ISBN (Electronic version): 978-94-034-0945-3

rijksuniversiteit
groningen

Dynamics Amidst Folding and Twisting in 2-Dimensional Maps

Proefschrift

ter verkrijging van de graad van doctor aan de
Rijksuniversiteit Groningen
op gezag van de
rector magnificus prof. dr. E. Sterken
en volgens besluit van het College voor Promoties.

De openbare verdediging zal plaatsvinden op

vrijdag 19 oktober 2018 om 16.15

door

Swier Harm Pieter Garst

geboren op 31 juli 1953
te Delft

Promotor
Prof. dr. H. Broer

Copromotores
Em. prof. dr. J. Aarts
Dr. A. Sterk

Beoordelingscommisie
Prof. dr. A. Jorba
Prof. dr. G.B. Huitema
Prof. dr. G.Vegter

Voor Jan Aarts

Contents

Chapter 1

Introduction

In the 1980's Hans Lauwerier (1923–1997) gave a keynote talk on dynamical systems at the Dutch Mathematical Congress in Delft. At the end of his talk he mentioned a 2-dimensional discrete-time predator-prey model and he showed the chaotic attractor in Figure 1.1 that he had detected in numerical experiments on his personal computer. This figure suggests that the dynamics of this predator-prey model can be understood in terms of the composition of a rotation and fold of the plane. Lauwerier's concluding remark was that there is still a lot of work to do in fully understanding the dynamics of this model. This formed the inspiration of the present work. The aim of this thesis is to provide a coherent overview of the dynamics of 2-dimensional iterated maps that exhibit folding and twisting using both analytical and numerical techniques. The present work is the result of a research project that started within the "Leraar in Onderzoek" program of the Netherlands Organisation for Scientific Research that aims at enabling mathematics teachers at secondary schools to participate in scientific research. The results presented in this thesis have been published in the form of two journal articles [12, 13].

1.1 Understanding dynamical systems

1.1.1 Studying geometric structures

The general background of the present work is formed by the mathematical theory of *dynamical systems* as it evolved since Henri Poincaré, Stephen Smale, René Thom, and many others. The general aim is to understand

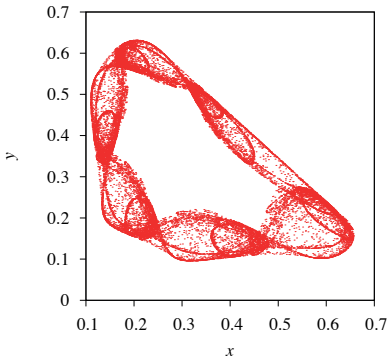

Figure 1.1. *Chaotic attractor of a planar, non-invertible map. This figure suggests that the map can be understood as the composition of a fold and a rotation.*

the long-term behaviour of nonlinear deterministic systems and qualitative changes in dynamics upon variation of parameters. The transition from orderly to complex chaotic dynamics is particularly important. Rather than studying individual evolutions, the goal is to obtain a global and qualitative overview of the dynamics by studying the geometric organisation of the product of state and parameter spaces.

An important problem in the theory of dynamical systems is to determine the geometric structure of chaotic attractors and the bifurcations leading to their formation. Inspiration for the development of the theory often comes from the analytical and numerical study of particular examples, but the goal is to understand the dynamics of a large class of systems. Ideally, one would like to classify the behavior of dynamical systems according to some equivalence relation. For example, dynamical systems that are topologically conjugate have identical topological properties, and in particular they share the same number of fixed points and periodic orbits of the same stability types. However, topological conjugacy can only be proved in specific cases.

In the vicinity of bifurcations one can use the theory of normal forms. All systems exhibiting a certain type of bifurcation are locally (i.e., around the

equilibrium) topologically equivalent to the normal form of the bifurcation [11, 14, 19].

A fruitful strategy to understand chaotic dynamics is to construct representative examples that explain the dynamical behavior observed in concrete applications. A well-known example is the *horseshoe map* introduced by Smale [28] which has become one of the hallmarks of chaos. The horseshoe map is an Axiom A diffeomorphism that serves as a model for the generic behavior at a transverse homoclinic point at which the stable and unstable manifolds of a periodic point intersect. Another example of this strategy is given by the so-called *geometric Lorenz models* that were constructed to understand the attractor of the Lorenz-63 system [1, 15, 29, 31]. Such *toy models*, or *models of models*, are of great help to understand complex dynamics.

In many works a similar strategy has been adopted to unravel generic dynamical features in the vicinity of particular bifurcations. A simplified global model for the return map of a dissipative diffeomorphism near a homoclinic bifurcation was presented in [5]. This map is a perturbation of the Arnold family of circle maps and its dynamics involves periodicity, quasi-periodicity and chaos, between which there are various transitions bifurcations. This map has a universal character in the setting of 2-dimensional diffeomorphisms and can be compared with examples like the Hénon map and the standard map.

Detailed studies of 3-dimensional diffeomorphisms, in particular near a Hopf-saddle-node bifurcation, can be found in [8, 9, 30]. These studies were mainly inspired by results obtained for the Poincaré map of the periodically driven Lorenz–84 atmospheric model [6]. In the latter map so-called quasi-periodic Hénon-like attractors, which are conjectured to coincide with the unstable manifold of a hyperbolic invariant circle of saddle-type, have been detected [7]. The existence of such attractors has been rigorously proved for a map on the solid torus [10].

1.1.2 Maps that fold and twist the plane

In this work we are concerned with the study of *non-invertible*, planar maps. The study of such maps goes back to at least the works of Gumowski and Mira [16, 17, 25] who studied the role of critical lines in the formation of basin boundaries and their bifurcations. Since the 1990s the interest for 2-dimensional endomorphisms has increased tremendously. For a detailed

account, the reader is referred to the textbook of Mira et al. [26] and the references therein.

The aim of this work is to understand the the dynamics of 2-dimensional maps that rotate and fold the plane. In accordance with the philosophy outlined above we will construct a *toy model* that is intended to serve as a representative example for this class of maps. The inspiration for this map is taken from two examples that appeared in the literature.

1.1.2.1 A predator-prey model

Consider for $x > 0$ and $y > 0$ the following planar map

$$\mathscr{P} : \begin{pmatrix} x \\ y \end{pmatrix} \mapsto \begin{pmatrix} ax(1-x-y) \\ bxy \end{pmatrix}. \tag{1.1}$$

This map is a simplification of the predator-prey model studied in [2]; also see [26] and references therein. It was precisely this map that was mentioned in Lauwerier's key note talk at the Dutch Mathematical Congress.

The map $\mathscr{P}$ folds the plane along the line $ab - 4bx - 4ay = 0$ and hence is not invertible. In the half-plane $ab - 4bx - 4ay > 0$ the map $\mathscr{P}$ has two preimages. Moreover, this map has a fixed point $(\frac{1}{b}, 1 - \frac{1}{a} - \frac{1}{b})$, which has complex eigenvalues for the parameters $b > (a + \sqrt{a})/(2a - 2)$. Hence, the map $\mathscr{P}$ rotates points near this fixed point.

1.1.2.2 A discretized Lorenz-63 model

Our second example arises from the classical Lorenz-63 model [21, 22] for Rayleigh-Bénard convection:

$$\frac{dx}{dt} = -\sigma(x - y), \qquad \frac{dy}{dt} = \rho x - y - xz, \qquad \frac{dz}{dt} = -\beta z + xy.$$

Taking the limit $\sigma \to \infty$ gives a system of two differential equations:

$$\frac{dy}{dt} = (\rho - 1)y - yz, \qquad \frac{dz}{dt} = -\beta z + y^2.$$

In what follows, we will relabel the variables (y, z) as (x, y) again. In this 2-dimensional system we can assume without loss of generality that $\beta = 1$ by a suitable rescaling (but note that this property does not hold for the

3-dimensional system). After discretizing these equations by means of a forward Euler scheme with time step τ we obtain the map

$$\mathscr{L} : \begin{pmatrix} x \\ y \end{pmatrix} \mapsto \begin{pmatrix} (1+\alpha\tau)x - \tau xy \\ (1-\tau)y + \tau x^2 \end{pmatrix}, \tag{1.2}$$

where $\alpha = \rho - 1$.

First note that the map $\mathscr{L}$ is noninvertible. The curve defined by the equation

$$4\tau(y - cb)^3 = 27c^2x^2, \quad c = 1 - \tau, \quad b = (1 + \alpha\tau)/\tau,$$

separates two regions in the plane in which the map has either one or three preimages. In addition, the map has a fixed point $(\pm\sqrt{\alpha}, \alpha)$ of which the eigenvalues are complex for $\alpha > \frac{1}{8}$, which means that points near the fixed point are rotated by the map.

1.2 Setting of the problem

1.2.1 Main research question

Considering the properties of the maps $\mathscr{P}$ and $\mathscr{L}$ the main research question can be formulated as: can a map be constructed which fundamentally describes the dynamics of maps with a fold and a twist.
In this work (see next subsection) the fold-and-twist map $\mathscr{F}$ is defined as an educated guess for the stated question. Then in [12] which is in Chapter 2 of this work, the dynamics of this fold-and-twist map is described. In Chapter 3 of this work, published in [13], the Lyapunov diagrams, the snap-back repellers and the folded Hénon-like attractors for the three maps $\mathscr{P}$, $\mathscr{L}$ and $\mathscr{F}$ are compared.

1.2.2 The fold-and-twist map

The maps $\mathscr{P}$ and $\mathscr{L}$ rotate points and fold the plane. Our aim is to study the combination of these effects in a representative toy model that is as simple as possible. To that end, we first define the map

$$\mathscr{F} : \begin{pmatrix} x \\ y \end{pmatrix} \mapsto \begin{pmatrix} f(x) \\ y \end{pmatrix},$$

where $f : \mathbb{R} \to \mathbb{R}$ is a continuous two-to-one map. Observe that $\mathscr{F}$ maps vertical lines onto vertical lines. In the following we will take

$$f(x) = \tfrac{1}{4}(a-2) - ax^2$$

which is conjugate to the logistic family $g(x) = ax(1-x)$. Indeed, for $\psi(x) = x - \frac{1}{2}$ we have that $f \circ \psi = \psi \circ g$. Hence, we will restrict to the parameter range $a \in [0, 4]$. Next, we consider a rigid rotation around the origin given by

$$\mathscr{R} : \begin{pmatrix} x \\ y \end{pmatrix} \mapsto \begin{pmatrix} x\cos\varphi - y\sin\varphi \\ x\sin\varphi + y\cos\varphi \end{pmatrix}.$$

The *fold-and-twist map* $\mathscr{T}$ is defined as the composition

$$\mathscr{T} = \mathscr{R} \circ \mathscr{F} : \begin{pmatrix} x \\ y \end{pmatrix} \mapsto \begin{pmatrix} f(x)\cos\varphi - y\sin\varphi \\ f(x)\sin\varphi + y\cos\varphi \end{pmatrix}. \tag{1.3}$$

The angle φ is measured in radians. However, for numerically obtained results values are reported in degrees, which is indicated by means of a subscript: $\varphi_d = 180\varphi/\pi$.

The dynamical properties of the map $\mathscr{T}$ were explored in [12]. The advantage of the map $\mathscr{T}$ is that the folding and twisting can be controlled separately using the parameters a and φ, and the philosophy of this work is that the map $\mathscr{T}$ may serve as a "guide" to study and explain phenomena that are observed in the maps $\mathscr{P}$ and $\mathscr{L}$.

1.3 Sketch of the results

The dynamics of the maps $\mathscr{P}$, $\mathscr{L}$, and $\mathscr{T}$ will be explored using both analytical and numerical tools. Sometimes educated guesses obtained from numerical explorations replace rigorous mathematical theorems, which is a way of thinking that is often referred to as *experimental mathematics*.

1.3.1 Lyapunov diagrams

The Lyapunov diagrams in Figure 1.2 show a classification of the dynamical behavior of the maps $\mathscr{P}$, $\mathscr{L}$, and $\mathscr{T}$ in different regions of their parameter planes. See Appendix B.1 for a description of the algorithm used to compute Lyapunov exponents. Note that the three diagrams have a very similar

geometric organization. In particular, one can observe a prevalence of periodic dynamics and chaotic dynamics. In all three diagrams one can observe tongue-shaped regions emanating along a curve. This suggests the presence of a Hopf–Neĭmark–Sacker bifurcation [11, 19].

The Lyapunov diagrams also suggest that chaotic attractors with one or two positive Lyapunov exponents occur for regions in the parameter plane with positive Lebesgue measure, and the question is how these attractors are formed and what their geometric structure is. Numerical evidence suggest that strange attractors having one positive Lyapunov exponent are of Hénon-like type, i.e., they are formed by the closure of the unstable manifold of a periodic point of saddle type. However, unlike in diffeomorphisms, these attractors have a folded structure in our maps.

1.3.2 Snap-back repellers

Providing rigorous proofs for the occurrence of chaotic dynamics in a dynamical system is often challenging. In 1975, Li and Yorke published their classical article in which they proved that the existence of a period-3 point implies chaos for interval maps [20]. This theorem inspired Marotto in 1978 to introduce the concept of a *snap-back repeller* as a sufficient condition for chaos in maps of higher dimensions [23]. Years later a technical flaw was discovered and Marotto published a revised definition of the snap-back repeller [24].

In what follows $\|\cdot\|$ denotes the standard Euclidean norm on $\mathbb{R}^n$ and $B_r(p) := \{x \in \mathbb{R}^n : \|x - p\| \leq r\}$ denotes a closed ball with radius r around the point p.

Definition 1 (Marotto [23, 24])**.** *Let $\mathscr{F} : \mathbb{R}^n \to \mathbb{R}^n$ be a differentiable map. A fixed point p of $\mathscr{F}$ is called a* snap-back repeller *if the following two conditions are satisfied:*

(i) the fixed point p is expanding*, which means that there exists an $r > 0$ such that the eigenvalues of $D\mathscr{F}(x)$ exceed 1 in absolute value for all $x \in B_r(p)$;*

(ii) there exists a point $x_0 \in B_r(p)$ with $x_0 \neq p$ and $m \in \mathbb{N}$ such that $x_m = p$ and $\det(D\mathscr{F}(x_k)) \neq 0$ for all $1 \leq k \leq m$ where $x_k = \mathscr{F}^k(x_0)$.

Invertible maps cannot have snap-back repellers. For these maps the occurrence of chaotic dynamics is often proved via the existence of bifurcations

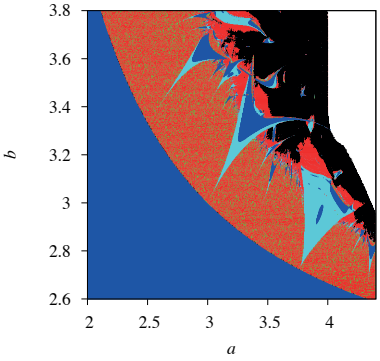

(a) *The map $\mathscr{P}$.*

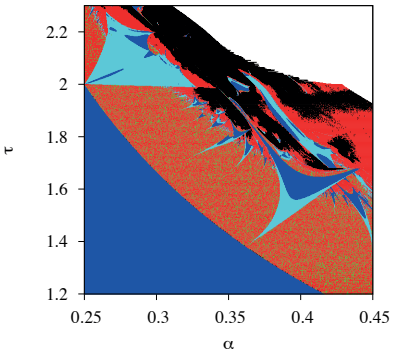

(b) *The map $\mathscr{L}$.*

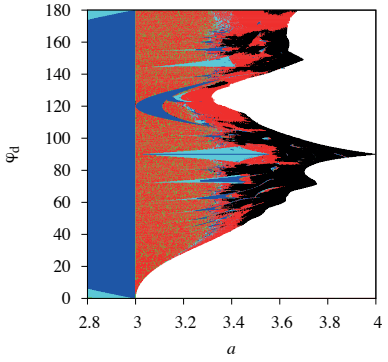

(c) *The map $\mathscr{T}$.*

Color	Lyapunov exponents	Attractor type
Cyan	$0 > \lambda_1 > \lambda_2$	per point of node type
Blue	$0 > \lambda_1 = \lambda_2$	per point of focus type
Green	$0 = \lambda_1 > \lambda_2$	invariant circle
Red	$\lambda_1 > 0 \geq \lambda_2$	chaotic attractor
Black	$\lambda_1 \geq \lambda_2 > 0$	chaotic attractor
White		no attractor detected

(d) *Color coding for the Lyapunov diagram of Figures 1.2a, 1.2b, and 1.2c. The diagrams suggest that periodic attractors and chaotic attractors with 1 or 2 positive Lyapunov exponents occur for regions in the parameter plane with positive Lebesgue measure.*

Figure 1.2. *Lyapunov diagram of attractors for the maps $\mathscr{P}$, $\mathscr{L}$, and $\mathscr{T}$ as a function of their parameters. For the color coding see Table 1.2d.*

that lead to homoclinic tangencies of stable and unstable manifolds of periodic points of saddle type, see Palis and Takens [27] for a general account. Marotto's theorem showed that the existence of a snap-back repeller is a sufficient condition for chaotic dynamics of *non-invertible* maps. Remarkably, this theorem only requires conditions on expanding periodic points and circumvents the computation of stable and unstable manifolds and their intersections. In this sense proving the occurrence of chaotic dynamics for noninvertible maps is easier than for invertible maps.

Figure 1.3 shows an example of snap-back repellers that have been numerically detected in the maps $\mathscr{P}$ and $\mathscr{T}$. For the map $\mathscr{T}$ the existence of snap-back repellers can be rigorously proved when $|\varphi - \pi/2|$ is sufficiently small.

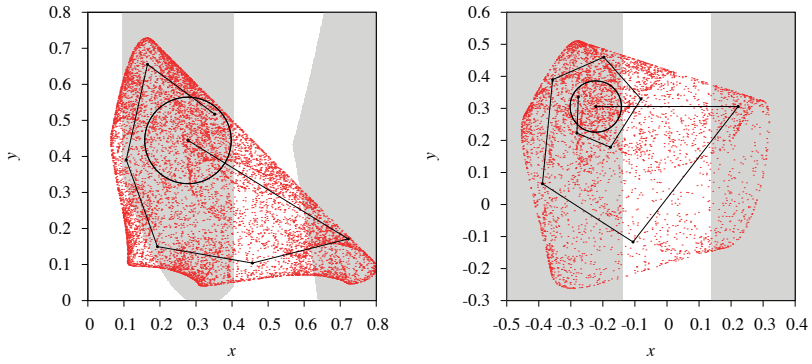

Figure 1.3. *Left panel: a chaotic attractor of the predator-prey map $\mathscr{P}$ for $(a, b) = (3.6, 3.6)$. The regions for which the Jacobian matrix of $\mathscr{P}$ has two unstable eigenvalues are indicated in grey. The point $(0.277778, 0.444444)$ is an expanding fixed point which is in fact a snap-back repeller: an orbit of length 6 of preimages (indicated with dots and line segments to guide the eye) of this point enters a ball of radius $r = 0.12$ around the fixed point. Right panel: a snap-back repeller for the map $\mathscr{T}$ with $(a, \varphi_d) = (3.6, 72)$, the fixed point $(-0.222222, 0.305863)$, $m = 9$, and $r = 0.08$.*

1.3.3 Folded Hénon-like attractors

The existence of a snap-back repeller only proves the existence of chaotic dynamics, but a central problem in the mathematical theory of dynamical systems is to also determine the *geometric structure* of chaotic attractors and the bifurcations leading to their formation. A classical example for which rigorous results are available is the well-known Hénon-map [18]. Benedicks and Carleson [3, 4] proved that there exists a set of positive measure in the parameter plane for which the Hénon map has a strange attractor which coincides with the closure of the unstable manifold of a saddle fixed point.

Detailed studies of the attractors in 3-dimensional diffeomorphisms, in particular near a Hopf-saddle-node bifurcation, can be found in [8, 9, 30]. These studies were mainly inspired by results obtained for the Poincaré map of the periodically driven Lorenz–84 atmospheric model [6]. In the latter map so-called quasi-periodic Hénon-like attractors, which are conjectured to coincide with closure of the unstable manifold of a saddle invariant circle, have been detected [7]. The existence of such attractors has been rigorously proved for a map on the solid torus [10].

Periodic attractors in the maps $\mathscr{P}$, $\mathscr{L}$, and $\mathscr{T}$ typically bifurcate through an infinite cascade of period doublings. Figure 1.4 present numerical evidence that the chaotic attractors detected near the end of this cascade are of Hénon-like type, which means that they are equal to the closure of the unstable manifold of a saddle periodic point. Note that strictly speaking, we must speak of an "unstable set" instead of an "unstable manifold". Indeed, since the maps $\mathscr{P}$, $\mathscr{L}$, and $\mathscr{T}$ are not diffeomorphisms the unstable set can have self-intersections which are indeed clearly visible in the aforementioned figures. An explanation of this phenomenon in terms of critical lines will be provided in Chapter 3.

1.4 Concluding remarks

The philosophy of introducing toy models is very useful to understand more complex dynamical systems. The fold-and-twist map $\mathscr{T}$ shares many dynamical features with the predator-prey map $\mathscr{P}$ and Lorenz' map $\mathscr{L}$. We have analytically proven the existence of a Hopf–Neĭmark–Sacker bifurcation, which gives rise to resonance tongues in the parameter plane of the map. Inside a resonance tongue a periodic attractor typically either under-

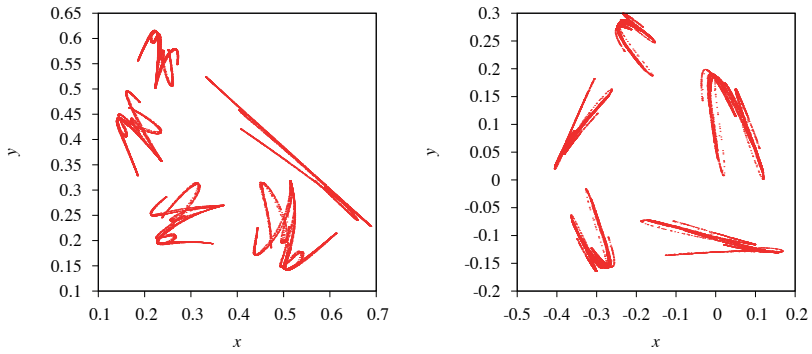

Figure 1.4. *Left panel: a chaotic attractor of the map $\mathscr{P}$ for the parameter values $(a, b) = (3.85, 3.2)$. Right panel: a chaotic attractor of the map $\mathscr{T}$ for the parameter values $(a, \varphi_d) = (3.43, 148)$. These attractors resemble a "fattened curve". In fact, numerical evidence suggests that these attractors are the closure of the unstable manifold of a saddle periodic point. Since the maps are non-invertible the unstable manifolds can have self-interections which can be explained by means of the concept of critical lines.*

goes a period doubling cascade, which leads to chaotic dynamics, or a another Hopf–Neĭmark–Sacker bifurcation, which in turn leads to a new family of tongues. For all maps we have detected chaotic attractors of Hénon-like type: these attractors are conjectured to be the closure of an unstable manifold of a saddle periodic point. Due to the non-invertibility of the map these attractors have a folded structure which can be explained by means of the iterates of the critical line. In addition, we have detected snap-back repellers which may coexist with Hénon-like attractors.

We conjecture that the dynamics described above is typical for planar maps that rotate and fold the plane. We even conjecture that the map $\mathscr{T}$ may serve as a *prototype* for such maps. The advantage of the map $\mathscr{T}$ is that the action of folding and rotation can be controlled separately through the parameters a and φ. In particular, for $\varphi = \pi/2$ we were able to analytically prove the existence of snap-back repellers for the fourth iterate of $\mathscr{T}$.

1.5 Further research

Note that our definition of $\mathscr{T}$ can also be used to consider more complicated non-invertible maps. For example, in (3.3) we can replace the function $f(x) = \frac{1}{4}(a-2) - ax^2$ by a function that has more than two preimages. A concrete example of such a map could be $f(x) = ax(x^2-1)$. Another choice for f would be the so-called tent map. In this case the fold-and-twist map $\mathscr{F}$ is not smooth, but it may be amenable to a more rigorous investigation. This approach is comparable to the Lozi map that was introduced to obtain a better understanding of the Hénon map.

Bibliography for Chapter 1

[1] V.S. Afraimovich, V.V. Bykov, and L.P. Shil'nikov. Origin and structure of the Lorenz attractor. *Akademiia Nauk SSSR Doklady*, 234:336–339, 1977.

[2] J.R. Beddington, C.A. Free, and J.H. Lawton. Dynamic complexity in predator-prey models framed as difference equations. *Nature*, 255:58–60, 1976.

[3] M. Benedicks and L. Carleson. On iterations of $1 - ax^2$ on $(-1, 1)$. *Annals of Mathematics*, 122:1–25, 1985.

[4] M. Benedicks and L. Carleson. The dynamics of the Hénon map. *Annals of Mathematics*, 133:73–169, 1991.

[5] H.W. Broer, C. Simó, and J.C. Tatjer. Towards global models near homoclinic tangencies of dissipative diffeomorphisms. *Nonlinearity*, 11:667–770, 1998.

[6] H.W. Broer, C. Simó, and R. Vitolo. Bifurcations and strange attractors in the Lorenz-84 climate model with seasonal forcing. *Nonlinearity*, 15:1205–1267, 2002.

[7] H.W. Broer, C. Simó, and R. Vitolo. Quasi-periodic hénon-like attractors in the Lorenz-84 climate model with seasonal forcing. In F. Dumortier, H.W. Broer, J. Mahwin, A. Vanderbauwhede, and S.M. Verduyn-Lunel, editors, *Equadiff 2003, Proceedings International Conference on Differential Equations, Hasselt 2003*, pages 714–719. World Scientific, 2005.

[8] H.W. Broer, C. Simó, and R. Vitolo. Hopf saddle-node bifurcation for fixed points of 3d-diffeomorphisms: Analysis of a resonance 'bubble'. *Physica D*, 237:1773–1799, 2008.

[9] H.W. Broer, C. Simó, and R. Vitolo. The Hopf-saddle-node bifurcation for fixed points of 3D-diffeomorphisms: the Arnol′d resonance web. *Bulletin of the Belgian Mathematical Society Simon Stevin*, 15:769–787, 2008.

[10] H.W. Broer, C. Simó, and R. Vitolo. Chaos and quasi-periodicity in diffeomorphisms of the solid torus. *Discrete and Continuous Dynamical Systems B*, 14:871–905, 2010.

[11] H.W. Broer and F. Takens. *Dynamical Systems and Chaos*, volume 172 of *Applied Mathematical Sciences*. Springer, 2010.

[12] S. Garst and A.E. Sterk. The dynamics of a fold-and-twist map. *Indagationes Mathematicae*, 27:1279–1304, 2016.

[13] S. Garst and A.E. Sterk. Periodicity and chaos amidst twisting and folding in 2-dimensional maps. Accepted for publication in *International Journal of Bifurcation and Chaos*, 2018.

[14] J. Guckenheimer and P. Holmes. *Nonlinear oscillations, dynamical systems and bifurcations of vector fields*, volume 42 of *Applied Mathematical Sciences*. Springer, 1983.

[15] J. Guckenheimer and R.F. Williams. Structural stability of Lorenz attractors. *Publications Mathématiques de l'Institut des Hautes Études Scientifiques*, 50:59–72, 1979.

[16] I. Gumowski and C. Mira. Sur un algorithme de détermination du domaine de stabilité d'un point d'une récurrence non linéaire du deuxième ordre à variables réelles. *Comptes Rendus Acad. Sc. Paris, Série A*, 260:6524–6527, 1965.

[17] I. Gumowski and C. Mira. Sensitivity problems related to certain bifurcations in nonlinear recurrences relations. *Automatica*, 5:303–317, 1969.

[18] M. Hénon. A two dimensional mapping with a strange attractor. *Communications in Mathematical Physics*, 50:69–77, 1976.

[19] Yu.A. Kuznetsov. *Elements of Applied Bifurcation Theory*, volume 112 of *Applied Mathematical Sciences*. Springer, third edition, 2004.

[20] T.-Y. Li and J.A. Yorke. Period three implies chaos. *The American Mathematical Monthly*, 82:985–992, 1975.

[21] E.N. Lorenz. Deterministic nonperiodic flow. *Journal of the Atmospheric Sciences*, 20:130–141, 1963.

[22] E.N. Lorenz. Computational chaos – a prelude to computational instability. *Physica D*, 35:299–317, 1989.

[23] F.R. Marotto. Snap-back repellers imply chaos in $\mathbb{R}^n$. *Journal of Mathematical Analysis and Applications*, 63:199–223, 1978.

[24] F.R. Marotto. On redefining a snap-back repeller. *Chaos, Solitons and Fractals*, 25:25–28, 2005.

[25] C. Mira. Détermination practique du domaine de stabilité d'un point d'équilibre d'une récurrence non linéaire du deuxième ordre à variables réelles. *Comptes Rendus Acad. Sc. Paris, Série A*, 261:5314–5317, 1964.

[26] C. Mira, L. Gardini, A. Barugola, and J.C. Cathala. *Chaotic Dynamics in Two-Dimensional Noninvertible Maps*. World Scientific Publishing, 1996.

[27] J. Palis and F. Takens. *Hyperbolicity and sensitive chaotic dynamics at homoclinic bifurcations*. Cambridge University Press, 1993.

[28] S. Smale. Differentiable dynamical systems. *Bulletin of the American Mathematical Society*, 73:747–817, 1967.

[29] M. Viana. What's new on Lorenz strange attractors? *The Mathematical Intelligencer*, 22(3):6–19, 2000.

[30] R. Vitolo, H.W. Broer, and C. Simó. Routes to chaos in the Hopf-saddle-node bifurcation for fixed points of 3D-diffeomorphisms. *Nonlinearity*, 23:1919–1947, 2010.

[31] R.F. Williams. The structure of the Lorenz attractor. *Publications Mathématiques de l'Institut des Hautes Études Scientifiques*, 50:72–99, 1979.

Chapter 2

The dynamics of a fold-and-twist map

2.1 Introduction

In this Chapter we study the dynamics of a planar endomorphism which is composed of a fold and a rigid rotation. We present both analytic computations and numerical experiments in which educated guesses are inspired by the available theory.

The construction of the fold-and-twist map is inspired by the maps $\mathscr{P}$ and $\mathscr{L}$ in equations (3.1) and (3.2) which rotate points and fold the plane. Our aim is to study the combination of these effects in a map that is as simple as possible. To that end, we first define the map

$$\mathscr{F}(x, y) = (f(x), y),$$

where f is a continuous two-to-one map. Observe that $\mathscr{F}$ maps vertical lines onto vertical lines. In the following we will take

$$f(x) = \tfrac{1}{4}(a-2) - ax^2$$

which is conjugate to the logistic family $g(x) = ax(1-x)$: for $\psi(x) = x - \frac{1}{2}$ we have that $f \circ \psi = \psi \circ g$. Hence, we will restrict our focus to the parameter range $a \in [0, 4]$. Next, we consider a rigid rotation around the origin given by

$$\mathscr{R}(x, y) = (x\cos\varphi - y\sin\varphi, x\sin\varphi + y\cos\varphi).$$

The fold-and-twist map $\mathscr{T}$, hereafter referred to as FAT, is defined as the composition

$$\mathscr{T}(x,y) = (\mathscr{R} \circ \mathscr{F})(x,y) = (f(x)\cos\varphi - y\sin\varphi, f(x)\sin\varphi + y\cos\varphi). \quad (2.1)$$

The angle φ is measured in radians. However, for numerically obtained results values are reported in degrees, which is indicated by means of a subscript: $\varphi_d = \varphi \cdot (180/\pi)$.

Lemma 1. *For $0 \leq \varphi \leq \pi$ the maps $\mathscr{T}_{\varphi,a}$ and $\mathscr{T}_{2\pi-\varphi,a}$ are conjugate.*

Proof. For $\varphi = 0$ and $\varphi = \pi$ the statement is trivial. For $0 < \varphi < \pi$ we define the map $\Psi(x,y) = (x,-y)$. A straightforward computation shows that $\mathscr{T}_{\varphi,a} \circ \Psi = \Psi \circ \mathscr{T}_{2\pi-\varphi,a}$. Note that this proof holds for any function f in equation (3.3). □

In particular, the preceding Lemma implies that the bifurcation diagram in the (φ, a)-plane is symmetric with respect to the line $\varphi = \pi$. Therefore, it suffices to study the family $\mathscr{T}_{\varphi,a}$ for $0 \leq \varphi \leq \pi$.

2.1.1 Overview of the dynamics

The Lyapunov diagram in Figure 2.1 shows a classification of the dynamical behaviour in different regions of the (φ, a)-plane. See Appendix B.1 for a description of the algorithm used to compute Lyapunov exponents. The diagram suggests that periodic dynamics occurs in regions in the (φ, a)-plane having positive Lebesgue measure. In particular, along the line $a = 3$ one can observe tongue-shaped regions with periodic dynamics. This already suggests that at $a = 3$ a fixed point loses stability through a Hopf–Neĭmark–Sacker bifurcation. Proposition 2 in Section 2.2.1 shows that this is indeed the case.

In addition, Figure 2.1 suggests that chaotic attractors with one positive or two positive Lyapunov exponents occur for regions in the (φ, a)-plane having positive Lebesgue measure, and the question is how these attractors are formed and what their geometric structure is. Numerical evidence suggest that strange attractors having one positive Lyapunov exponent are of Hénon-like type, i.e., they are formed by the closure of the unstable manifold of a periodic point of saddle type. However, unlike in diffeomorphisms, the attractors in our map have a folded structure.

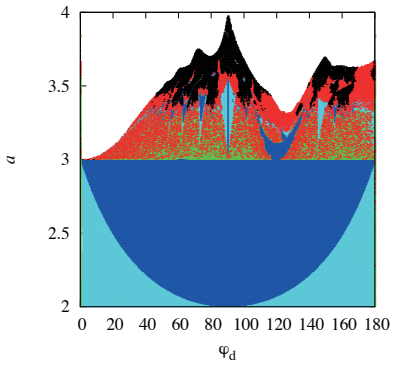

Figure 2.1. *Lyapunov diagram for the attractors of the map $\mathscr{T}_{\varphi,a}$. See Table 2.1 for the colour coding.*

2.2 Analytical results

The Lyapunov diagram suggests an abundance of periodic attractors. In this section we analytically prove the existence of such attractors and their bifurcations for special values of the parameters (φ, a).

2.2.1 Fixed points and their stability

The simplest attractors are those consisting of a single point. As explained in Appendix A.1 the stability of periodic points can be easily determined from the trace and determinant. The following Lemma is helpful.

Lemma 2. *A fixed point (x, y) of the map $\mathscr{T}_{\varphi,a}$ with $0 < \varphi < \pi$ is stable if and only if $-1 < -2ax < 1$.*

Proof. The determinant and trace of the Jacobian matrix of $\mathscr{T}_{\varphi,a}$ are given by $D = f'(x)$ and $T = (1 + f'(x)) \cos\varphi$. Equation (A.1) implies that a fixed point (x, y) is stable if and only if

$$-1 < f'(x) < 1 \quad \text{and} \quad -(1 + f'(x)) < (1 + f'(x)) \cos\varphi < (1 + f'(x)).$$

Since $-1 < \cos\varphi < 1$ the second inequality is satisfied without any further condition. The proof is completed by recalling that $f'(x) = -2ax$. □

Colour	Lyapunov exponents	Attractor type
cyan	$0 > \lambda_1 > \lambda_2$	periodic point of node type
blue	$0 > \lambda_1 = \lambda_2$	periodic point of focus type
green	$0 = \lambda_1 > \lambda_2$	invariant circle
red	$\lambda_1 > 0 \geq \lambda_2$	chaotic attractor
black	$\lambda_1 \geq \lambda_2 > 0$	chaotic attractor
white		no attractor detected

Table 2.1. *Colour coding for the Lyapunov diagram of Figure 2.1. The diagram suggests that periodic attractors and chaotic attractors with 1 or 2 positive Lyapunov exponents occur for regions in the (φ, a)-plane with positive Lebesgue measure.*

The next Proposition shows that the map $\mathscr{T}_{\varphi,a}$ has precisely two fixed points and explains how their stability changes by varying the parameters (φ, a).

Proposition 1. *For $a > 0$ and $0 < \varphi < \pi$ the map $\mathscr{T}_{\varphi,a}$ has two fixed points given by*

$$F_1 = \left(\frac{1}{2}, -\frac{1}{2}\cot\tfrac{1}{2}\varphi\right) \quad \textit{and} \quad F_2 = \left(\frac{2-a}{2a}, -\frac{2-a}{2a}\cot\tfrac{1}{2}\varphi\right).$$

Moreover, F_1 is stable for $0 \leq a < 1$ and F_2 is stable for $1 < a < 3$. In particular, F_1 and F_2 coalesce and exchange stability in a transcritical bifurcation at $a = 1$.

Proof. Fixed points of the fold-and-twist satisfy the equations

$$\begin{aligned} f(x)\cos\varphi - y\sin\varphi &= x \\ f(x)\sin\varphi + y\cos\varphi &= y \end{aligned}$$

which, for $0 < \varphi < 2\pi$, implies that

$$y = f(x)\frac{\sin\varphi}{1-\cos\varphi} = f(x)\cot(\tfrac{1}{2}\varphi) \quad \text{and} \quad f(x) = -x.$$

For $0 < a < 4$ the equation $f(x) = -x$ has the solutions $x = 1/2$ and $x = (2-a)/2a$ so that the fixed points of $\mathscr{T}_{\varphi,a}$ are given by

$$F_1 = \left(\frac{1}{2}, -\frac{1}{2}\cot\tfrac{1}{2}\varphi\right) \quad \text{and} \quad F_2 = \left(\frac{2-a}{2a}, -\frac{2-a}{2a}\cot\tfrac{1}{2}\varphi\right).$$

Note that F_1 and F_2 coincide for $a = 1$. Lemma 2 shows that F_1 is stable if and only if $-1 < a < 1$ and F_2 is stable if and only if $1 < a < 3$. This completes the proof. □

The next objects in terms of dynamical complexity are invariant circles on which the dynamics can be periodic or quasi-periodic. The existence of such circles for the map $\mathscr{T}_{\varphi,a}$ is implied by the next result.

Proposition 2. *For $0 < \varphi < \pi$ and $\varphi \neq 2\pi/3, \pi/2$ the fixed point F_2 loses stability through a supercritical Hopf–Neĭmark–Sacker (HNS) bifurcation at $a = 3$ and gives birth to a unique stable, closed invariant circle.*

Proof. Evaluating the Jacobian matrix of the map $\mathscr{T}_{\varphi,a}$ at the fixed point F_2 gives the matrix

$$J = \begin{pmatrix} (a-2)\cos\varphi & -\sin\varphi \\ (a-2)\sin\varphi & \cos\varphi \end{pmatrix},$$

which implies that $\det(J) = a - 2$ and $\mathrm{tr}(J) = (a-1)\cos\varphi$. From equation (A.1) it follows that the fixed point is stable if and only if $1 < a < 3$. Along the line $a = 3$ the fixed point loses stability as a complex conjugate pair of eigenvalues crosses the unit circle with nonzero speed. At the HNS bifurcation the eigenvalues are simply given by $\lambda_\pm = e^{\pm i\varphi}$. It immediately follows that the strong resonances occur for $\varphi \in \{\pi/2, 2\pi/3, \pi\}$.

We use equation (A.4) with $a_{11} = \cos\varphi$, $a_{12} = -\sin\varphi$, and $a_{21} = \sin\varphi$. Computations with the computer algebra package Mathematica then gives the following normal form coefficients:

$$h_{20} = 3e^{i\varphi}\sin\varphi, \quad h_{11} = 3e^{i\varphi}\sin\varphi, \quad h_{02} = 3e^{i\varphi}\sin\varphi, \quad h_{21} = 0,$$

so that the first Lyapunov coefficient is given by

$$\ell_1 = -\frac{27}{2}\sin^2\varphi.$$

Clearly, $\ell_1 < 0$ for $0 < \varphi < \pi$. Applying Theorem 4.6 of [34] implies that a unique stable, closed invariant curve bifurcates from the fixed point F_2 as a passes through 3. This completes the proof. □

Along the line $a = 3$ the eigenvalues of the fixed point F_2 are given by $\lambda_\pm = e^{\pm i\varphi}$. Hence, from points of the form $(\varphi, a) = (2\pi p/q, 3)$ with $p, q \in \mathbb{N}$ so-called Arnold tongues will emanate, which are indeed clearly visible in the

Lyapunov diagram of Figure 2.1. The boundaries of these tongues are formed by two saddle-node bifurcations, and for parameter values within a tongue a stable periodic point coexists with a saddle periodic point. In this case the invariant circle is formed by the unstable manifold of the saddle point, see Figure 2.2 for a numerical illustration near the 1:5 resonance tongue.

The points $(\varphi, 3)$ with $\varphi \in \{2\pi, \pi, 2\pi/3, \pi/2\}$ correspond to so-called strong resonances. For such parameter values more than one closed invariant curve can appear, or such a curve may not exist at all [34]. However, numerical evidence, which is presented in Figure 2.3, clearly suggests that in our case the invariant circle does exist for $\varphi = \pi/2$.

When changing the parameters (φ, a), the invariant circle can be destroyed by homoclinic tangencies between the stable and unstable manifolds of the unstable periodic point, or the circle can interact with other objects via heteroclinic tangencies. See [11, 12] for an extensive discussion.

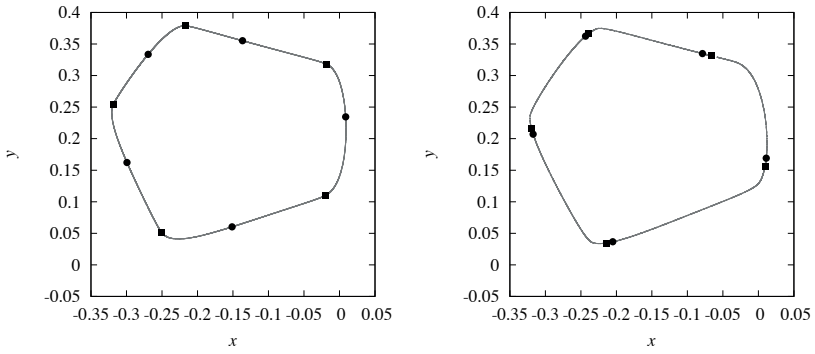

Figure 2.2. *For $a = 3.2$ and $\varphi_d = 73$ (left) and $\varphi_d = 73.8$ (right) a stable period-5 point (circles) coexists with a saddle period-5 point (squares). The unstable manifold of the saddle forms an invariant circle. Observe that for increasing φ the two periodic orbits will coalesce in a saddle-node bifurcation which forms one of the boundaries of the 1:5 resonance tongue.*

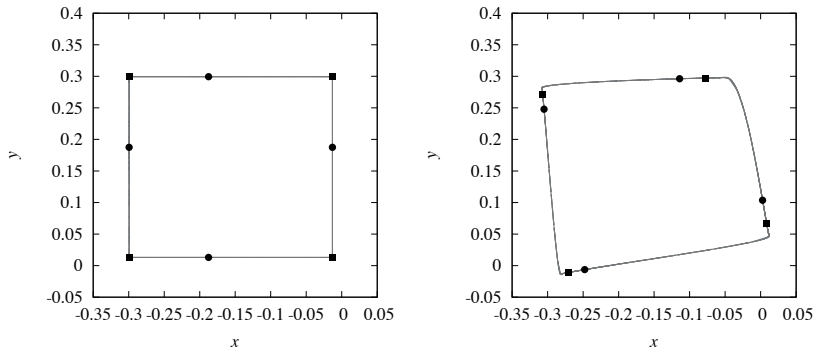

Figure 2.3. *As Figure 2.2, but for period 4 and parameters* $(\varphi_d, a) = (90, 3.2)$ *(left) and* $(\varphi_d, a) = (92, 3.2)$ *(right).*

2.2.2 Period-4 orbits for $\varphi = \pi/2$

For the special angle $\varphi = \pi/2$ the periodic point born at the HNS bifurcation described in Proposition 2 can be explicitly computed.

Proposition 3. *For* $\varphi = \pi/2$ *and* $a > 3$ *the map* $\mathscr{T}_{\varphi,a}$ *has two period-4 orbits given by*

$$P_1^{(4)} = (p_+, -p_+) \mapsto (p_+, -p_-) \mapsto (p_-, -p_-) \mapsto (p_-, -p_+),$$
$$P_2^{(4)} = (q, -p_-) \mapsto (p_-, -q) \mapsto (q, -p_+) \mapsto (p_+, -q),$$

where

$$p_\pm = \frac{-1 \pm \sqrt{(a-3)(a+1)}}{2a} \quad \textit{and} \quad q = \frac{2-a}{2a}.$$

The point $P_1^{(4)}$ *loses stability at* $a = 1 + \sqrt{6}$ *as two Floquet multipliers pass through* -1*. The point* $P_2^{(4)}$ *is unstable. At* $a = 3$ *they both coalesce with the fixed point* F_2*.*

Proof. Recall that $f(x) = \frac{1}{4}(a-2) - ax^2$. Since $f(x) = f(-x)$ we have

$$\mathscr{T}^4_{a,\pi/2}(x, y) = (-f(f(x)), f(f(y))).$$

Therefore, the period-4 points of $\mathscr{T}_{a,\pi/2}$ and their stability follow immediately from the fixed points of f^2 and $-f^2$. For $3 < a < 4$ the fixed points for $-f^2$ are given by

$$p_1 = \frac{1}{2}, \quad p_2 = \frac{2-a}{2a}, \quad p_3 = \frac{-1-\sqrt{(a-3)(a+1)}}{2a}, \quad p_4 = \frac{-1+\sqrt{(a-3)(a+1)}}{2a}.$$

Note that p is a fixed point of $-f^2$ if and only if $-p$ is a fixed point of f^2. Hence, there are 16 candidates for a period-4 point which are given by $(p_i, -p_j)$ for $1 \leq i, j \leq 4$. The Floquet multipliers are given by

$$\lambda_1 = -4a^2 p_i f(p_i) \qquad \text{and} \qquad \lambda_2 = -4a^2 p_j f(p_j).$$

Straightforward computations reveal that:

- $(p_1, -p_1)$ and $(p_2, -p_2)$ are fixed points.
- $(p_1, -p_2) \mapsto (p_2, -p_1)$ is an unstable period-2 orbit.
- $(p_1, -p_3) \mapsto (p_3, -p_1) \mapsto (p_1, -p_4) \mapsto (p_4, -p_1)$ is a period-4 orbit with Floquet multipliers $\lambda_1 = a^2$ and $\lambda_2 = 1 - (a-3)(a+1)$. Since $a > 3$ the orbit is unstable.
- $(p_2, -p_3) \mapsto (p_3, -p_2) \mapsto (p_2, -p_4) \mapsto (p_4, -p_2)$ is a period-4 orbit with Floquet multipliers $\lambda_1 = (2-a)^2$ and $\lambda_2 = 1 - (a-3)(a+1)$. Since $a > 3$ the orbit is unstable.
- $(p_4, -p_4) \mapsto (p_4, -p_3) \mapsto (p_3, -p_3) \mapsto (p_3, -p_4)$ is a period-4 orbit with Floquet multipliers $\lambda_1 = \lambda_2 = 1 - (a-3)(a+1)$. Note that $|\lambda_{1,2}| < 1$ for $3 < a < 1 + \sqrt{6}$, and at $a = 1 + \sqrt{6}$ the multipliers pass through -1.

Note that the periodic points $(p_2, -p_3)$ and $(p_4, -p_4)$ coalesce in a saddle-node bifurcation at $a = 3$. This completes the proof. □

Note that for $a = 3$ the periodic points $P_1^{(4)}$ and $P_2^{(4)}$ both have *two* Floquet multipliers equal to one, since the two saddle-node bifurcation curves forming the boundaries of the 1:4 tongue join in a cusp at the point $(\pi/2, 3)$. The unstable manifold of the saddle point $P_2^{(4)}$ forms an invariant circle for parameter values sufficiently close to the origin of the tongue; see Figure 2.3 for an illustration.

2.2.3 Period-3 orbits for $\varphi = 2\pi/3$

For the special angle $\varphi = 2\pi/3$ there exist two period-3 orbits which are *not* related to the HNS bifurcation described in Proposition 2. In fact, these period-3 orbits already exist for parameter values $a < 3$.

Proposition 4. *For $\varphi = 2\pi/3$ the map $\mathscr{T}_{\varphi,a}$ has two period-3 orbits given by*

$$P_{\pm}^{(3)} = \left(\frac{-1 \pm \sqrt{\Delta}}{6a}, \frac{(-5 \mp 7\sqrt{\Delta})\sqrt{3}}{54a}\right) \mapsto \left(\frac{-1 \pm \sqrt{\Delta}}{6a}, \frac{(19 \mp 5\sqrt{\Delta})\sqrt{3}}{54a}\right) \mapsto \left(\frac{-5 \mp \sqrt{\Delta}}{6a}, \frac{(7 \mp \sqrt{\Delta})\sqrt{3}}{54a}\right),$$

where $\Delta = 9a^2 - 18a - 23$. The point $P_+^{(3)}$ is stable for $a_0 < a < a_1$, where

$$a_0 = \tfrac{1}{3}(3 + 4\sqrt{2}) \approx 2.85 \qquad \text{and} \qquad a_1 = 1 + \tfrac{1}{6}\sqrt{174 - 6\sqrt{5}} \approx 3.11.$$

At $a = a_0$ the points $P_{\pm}^{(3)}$ coalesce in a saddle-node bifurcation and at $a = a_1$ the point $P_+^{(3)}$ loses stability as two Floquet multipliers cross the unit circle. The point $P_-^{(3)}$ is unstable for all $a > a_0$.

Proof. In this section we fix $\varphi = 2\pi/3$. We have that $(x_{i+1}, y_{i+1}) = \mathscr{T}(x_i, y_i)$ if and only if

$$\begin{aligned} f(x_i) &= -\tfrac{1}{2}x_{i+1} + \tfrac{1}{2}\sqrt{3}y_{i+1}, \\ y_i &= -\tfrac{1}{2}\sqrt{3}x_{i+1} + \tfrac{1}{2}y_{i+1}. \end{aligned}$$

Therefore, the points (x_1, y_1), (x_2, y_2), and (x_3, y_3) form a period-3 orbit if and only if the following equations are satisfied:

$$\begin{aligned} f(x_1) &= -\tfrac{1}{2}x_2 + \tfrac{1}{2}\sqrt{3}y_2, \\ f(x_2) &= -\tfrac{1}{2}x_3 + \tfrac{1}{2}\sqrt{3}y_3, \\ f(x_3) &= -\tfrac{1}{2}x_1 + \tfrac{1}{2}\sqrt{3}y_1, \\ y_1 &= -\tfrac{1}{2}\sqrt{3}x_2 + \tfrac{1}{2}y_2, \\ y_2 &= -\tfrac{1}{2}\sqrt{3}x_3 + \tfrac{1}{2}y_3, \\ y_3 &= -\tfrac{1}{2}\sqrt{3}x_1 + \tfrac{1}{2}y_1. \end{aligned}$$

The last three equations are linear in the variables y_i, and therefore we can use Cramer's rule to express the y-coordinates in terms of the x-coordinates:

$$\begin{aligned} y_1 &= -\frac{\sqrt{3}}{9}(4x_2 - 2x_3 + x_1), \\ y_2 &= -\frac{\sqrt{3}}{9}(4x_3 - 2x_1 + x_2), \\ y_3 &= -\frac{\sqrt{3}}{9}(4x_1 - 2x_2 + x_3). \end{aligned} \tag{2.2}$$

Substituting this in the first three equations gives the following equations for the x-coordinates:

$$\begin{aligned} 3f(x_1) &= x_1 - 2x_2 - 2x_3, \\ 3f(x_2) &= x_2 - 2x_1 - 2x_3, \\ 3f(x_3) &= x_3 - 2x_1 - 2x_2. \end{aligned}$$

By substituting $f(x) = \frac{1}{4}(a-2) - ax^2$, multiplying the equations by $12a$, and setting $u_i = 6ax_i + 1$ we can rewrite these equations as

$$\begin{aligned} u_1^2 - 4u_2 - 4u_3 &= 9a^2 - 18a - 7, \\ u_2^2 - 4u_1 - 4u_3 &= 9a^2 - 18a - 7, \\ u_3^2 - 4u_1 - 4u_2 &= 9a^2 - 18a - 7. \end{aligned}$$

Subtracting the second equation from the first gives $(u_1+2)^2 = (u_2+2)^2$ which implies that

$$u_2 = u_1 \qquad \text{or} \qquad u_2 = -(u_1 + 4).$$

Subtracting the third equation from the second gives $(u_2+2)^2 = (u_3+2)^2$ which implies that

$$u_3 = u_2 \qquad \text{or} \qquad u_3 = -(u_2 + 4).$$

This gives four different quadratic equations for u_1.

(i) If $u_1 = u_2 = u_3$, then $x_1 = x_2 = x_3$. Equations (2.2) then imply that $y_1 = y_2 = y_3$. Hence, in this case we do not obtain a period-3 orbit, but a fixed point.

(ii) For $u_2 = u_1$ and $u_3 = -(u_2 + 4)$ we obtain the equation

$$u_1^2 = 9a^2 - 18a - 23.$$

(iii) For $u_2 = -(u_1 + 4)$ and $u_3 = u_2$ we obtain the equation

$$(u_1 + 4)^2 = 9a^2 - 18a - 23.$$

In this case we obtain the same period-3 orbits as in case (ii).

(iv) For $u_2 = -(u_1 + 4)$ and $u_3 = -(u_2 + 4)$ we again obtain the equation

$$u_1^2 = 9a^2 - 18a - 23.$$

In this case we obtain the same period-3 orbits as in case (ii).

Setting $\Delta = 9a^2 - 18a - 23$ we obtain from case (ii) the solutions

$$u_1 = \pm\sqrt{\Delta}, \quad u_2 = \pm\sqrt{\Delta}, \quad u_3 = -4 \mp \sqrt{\Delta}.$$

This gives the two period-3 orbits

$$\begin{aligned}
(x_1, y_1) &= \left(\frac{-1 \pm \sqrt{\Delta}}{6a}, \frac{(-5 \mp 7\sqrt{\Delta})\sqrt{3}}{54a} \right), \\
(x_2, y_2) &= \left(\frac{-1 \pm \sqrt{\Delta}}{6a}, \frac{(19 \mp 5\sqrt{\Delta})\sqrt{3}}{54a} \right), \\
(x_3, y_3) &= \left(\frac{-5 \mp \sqrt{\Delta}}{6a}, \frac{(7 \mp \sqrt{\Delta})\sqrt{3}}{54a} \right).
\end{aligned}$$

These orbits exist only for $\Delta \geq 0$ which is the case for $a \leq a_-$ and $a \geq a_+$ where $a_\pm = \frac{1}{3}(3 \pm 4\sqrt{2})$. At $a = a_\pm$ the orbits coalesce in a saddle-node bifurcation. Since $a_- < 0$ we only consider the case $a \geq a_+$.

The Jacobian matrix of $\mathscr{T}^3$ evaluated at (x_1, y_1) is given by

$$J = \begin{pmatrix} ax_3 & -\frac{1}{2}\sqrt{3} \\ -a\sqrt{3}x_3 & -\frac{1}{2} \end{pmatrix} \begin{pmatrix} ax_2 & -\frac{1}{2}\sqrt{3} \\ -a\sqrt{3}x_2 & -\frac{1}{2} \end{pmatrix} \begin{pmatrix} ax_1 & -\frac{1}{2}\sqrt{3} \\ -a\sqrt{3}x_1 & -\frac{1}{2} \end{pmatrix}$$

Its determinant and trace are respectively given by

$$\begin{aligned}
D &= -8a^3 x_1 x_2 x_3, \\
T &= \frac{1}{8}(-1 + 8a^3 x_1 x_2 x_3 + 12a^2(x_1 x_2 + x_2 x_3 + x_1 x_3) - 6a(x_1 + x_2 + x_3)).
\end{aligned}$$

We investigate the stability for the two periodic orbits seperately.

For the period-3 orbit obtained for the positive sign we have that $D = p_+(\sqrt{\Delta})$ and $T = q_+(\sqrt{\Delta})$ where

$$p_+(t) = \frac{1}{27}\big(5 - 9t + 3t^2 + t^3\big) \quad \text{and} \quad q_+(t) = \frac{1}{216}\big(256 - 108t - 12t^2 - t^3\big).$$

Solving $p_+(t) = 1$ for $t \geq 0$ gives $t = \frac{1}{2}(-1 + 3\sqrt{5})$. Clearly, $q_+(t)$ decreases for $t \geq 0$. Moreover we have that

$$q(0) = 1 + p(0),$$
$$q(\tfrac{1}{2}(-1 + 3\sqrt{5}) = \tfrac{1}{8}(7 - 6\sqrt{5}) < -2 = -1 - p(\tfrac{1}{2}(-1 + 3\sqrt{5}).$$

This means that for $0 < t < \frac{1}{2}(-1 + 3\sqrt{5})$ we have that

$$-1 < p_+(t) < 1 \quad \text{and} \quad -1 - p_+(t) < q_+(t) < 1 + p_+(t).$$

We conclude that for $\frac{1}{3}(3 + 4\sqrt{2}) < a < 1 + \frac{1}{6}\sqrt{174 - 6\sqrt{5}}$ we have that

$$-1 < D < 1 \quad \text{and} \quad -1 - D < T < 1 + D,$$

so that equation (A.1) implies that the orbit is stable. At the critical value $a = 1 + \frac{1}{6}\sqrt{174 - 6\sqrt{5}}$ the periodic orbit loses stability as the line $D = 1$ is crossed, which means that two complex eigenvalues cross the unit circle.

Choosing the negative sign gives that $D = p_-(\sqrt{\Delta})$ and $T = q_-(\sqrt{\Delta})$ where

$$p_-(t) = \frac{1}{27}\big(5 + 9t + 3t^2 - t^3\big) \quad \text{and} \quad q_-(t) = \frac{1}{216}\big(256 + 108t - 12t^2 + t^3\big).$$

Note that

$$q_-(t) - (1 + p_-(t)) = \frac{t(t-2)^2}{24},$$

for all $t \geq 0$, which implies that

$$T \geq 1 + D$$

for all $a \geq a_+$ so that the orbit is unstable. This completes the proof. □

In particular, Propositions 1 and 4 imply that for $\varphi = 2\pi/3$ and $\frac{1}{3}(3 + 4\sqrt{2}) < a < 3$ the stable fixed point F_2 coexists with the stable period-3 point $P_+^{(3)}$. Figure 2.4 shows their basin of attraction for $a = 2.886$ and $a = 2.95$. As the parameter a approaches the value $a_{HNS} = 3$ the basin of attraction of the fixed point becomes smaller.

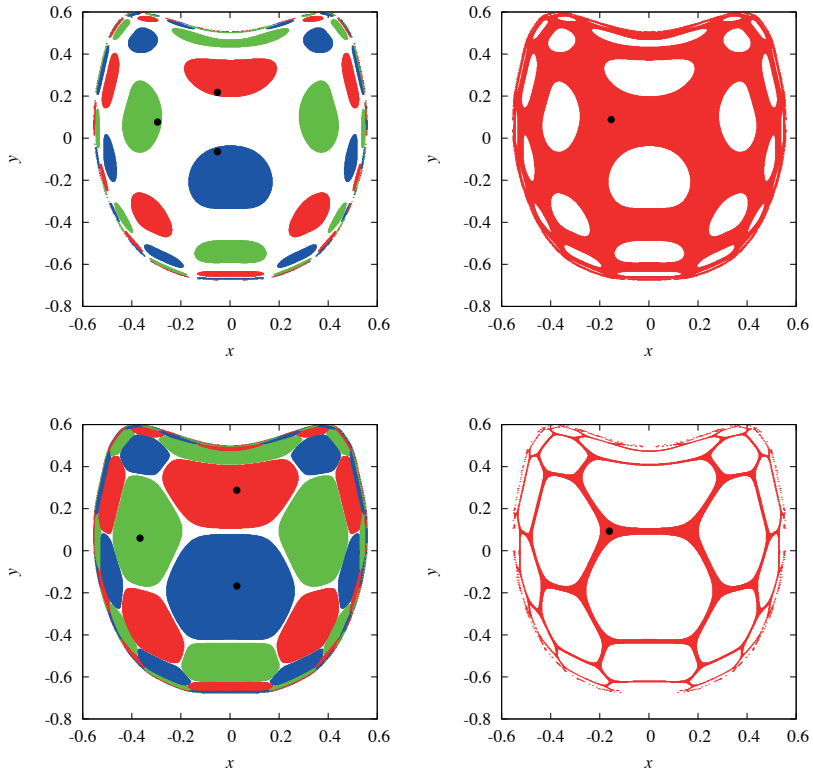

Figure 2.4. *For $\varphi = 2\pi/3$ and $\frac{1}{3}(3+4\sqrt{2}) < a < 3$ a stable period-3 point coexists with a fixed point. Top panels: the basins of attraction of the period-3 point (left) and the fixed point (right) for $a = 2.886$. Bottom panels: the same basins, but for $a = 2.95$. Note that the basin of the fixed point becomes smaller as the parameter a approaches the value 3.*

2.2.4 Critical manifolds

The critical manifold [43, 44] is an important tool in the study of non-invertible maps. We define the set

$$LC_{-1} = \{(x, y) \in \mathbb{R}^2 \,:\, \det D\mathscr{T}(x, y) = 0\} = \{(x, y) \in \mathbb{R}^2 \,:\, x = 0\}.$$

The critical line (French: "ligne critique") of the fold-and-twist map is defined as

$$LC = \mathscr{T}_{\varphi,a}(LC_{-1}) = \{(x,y) \in \mathbb{R}^2 \,:\, x\cos\varphi + y\sin\varphi = \tfrac{1}{4}(a-2)\}.$$

The line LC separates the following regions in the plane:

$$\begin{aligned} Z_0 &= \{(x,y) \in \mathbb{R}^2 \,:\, x\cos\varphi + y\sin\varphi > \tfrac{1}{4}(a-2)\}, \\ Z_2 &= \{(x,y) \in \mathbb{R}^2 \,:\, x\cos\varphi + y\sin\varphi < \tfrac{1}{4}(a-2)\}. \end{aligned}$$

Points in Z_0 have no preimage under $\mathscr{T}$, and points in Z_2 have two preimages under $\mathscr{T}$. In the terminology of Mira et al. [44] the fold-and-twist map $\mathscr{T}$ is of $Z_0 - Z_2$ type. For all parameters (φ, a) the map remains of this type. In particular, foliation bifurcations, as described in Mira's book, do not occur. The critical line LC and its iterates play an important role in the bifurcations of basin boundaries and in bounding invariant regions.

2.3 The dynamics near Arnold tongues

In this section we numerically study the dynamics of the FAT in and outside the Arnold tongues. We particularly focus on bifurcations of periodic points and their basins and the geometrical structure of chaotic attractors. For purposes of illustration we restrict the discussion to tongues of order 1:4, 1:5, 1:6, and 2:5, which have the largest size in the sense of Lebesgue measure. Similar dynamics is expected to be found near the other tongues.

2.3.1 Basins of attraction of periodic points

In this section we study the geometry of the basins of attraction of stable periodic points and the possible bifurcations of these basins. Unlike for diffeomorphisms, basins of attractions in noninvertible maps need not be simply connected [44].

Basin bifurcations in the 1:6 tongue. Figure 2.5 shows magnifications of the Lyapunov diagram of Figure 2.1 near the 1:6 resonance tongue. Within this tongue a stable period-6 attractor exists. Figure 2.6 shows basins of attraction of this attractor for $\varphi_d = 62.70$ and several values of a.

For $a = 3.35$ the basin for each point along the period-6 orbit is disconnected. Indeed, the magnification in Figure 2.6 suggests that the basin for each point consists of infinitely many components. We define the *immediate basin* to be the largest connected component which contains the attracting fixed point under $\mathscr{T}^6$. For $a = a_c$, with $3.36 < a_c < 3.37$, a contact bifurcation between the critical line LC and the boundary of a basin takes place. After this bifurcation the immediate basins become multiply connected as they are filled with islands which are part of the basin of another fixed point. As a increases the number of islands increases leading to a fractalization of the basin boundaries.

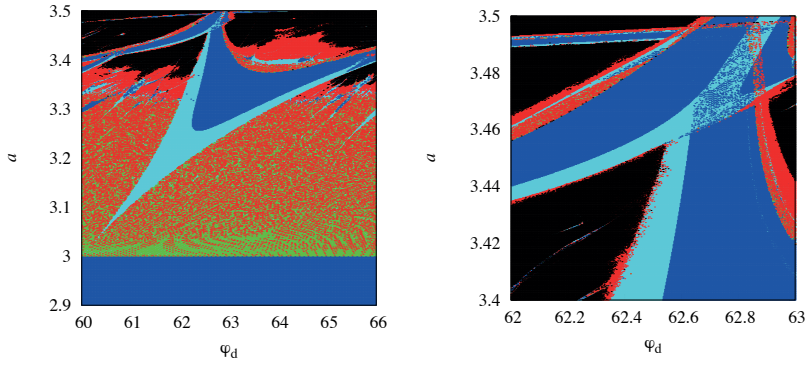

Figure 2.5. *Left: magnification of Lyapunov diagram in Figure 2.1 near the 1:6 resonance tongue. Right: magnification showing the overlap of the 1:6 and 1:7 tongues. See Table 2.1 for the colour coding.*

Coexistence of period-6 and period-7 attractors. The parameter values $(\varphi_d, a) = (62.7, 3.57)$ belong to both the 1:6 tongue and the 1:7 tongue, see Figure 2.5. For these parameter values we detected a stable period-6 point $(-0.368, 0.270)$ having complex Floquet multipliers $-0.52 \pm 0.45i$ and a stable period-7 point $(-0.423, 0.130)$ having real Floquet multipliers -0.16 and -0.91. Figure 2.7 shows the basin of attraction of each of these periodic attractors. Observe that the basin of the period-7 point occupies a much larger part of the (x, y)-plane than the basin of the period-6 point.

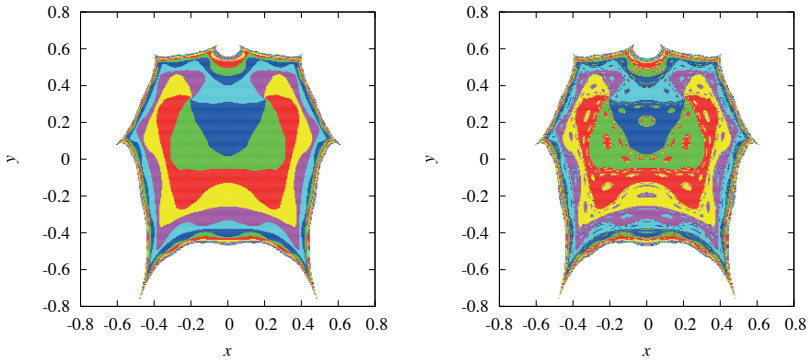

Figure 2.6. *Bifurcations of the basin of attraction of a period-6 attractor for the parameter values* $\varphi_d = 62.7$ *and* $a = 3.35$ *(left) and* $a = 3.37$ *(right).*

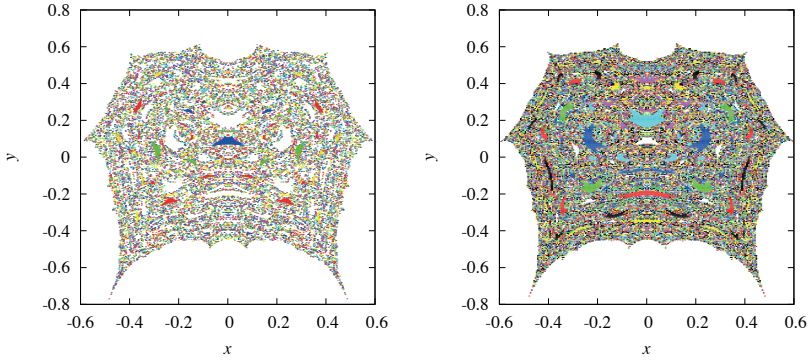

Figure 2.7. *For* $(\varphi_d, a) = (62.7, 3.57)$ *the 1:6 and 1:7 Arnold tongues overlap (see Figure 2.5) which leads to the coexistence of a period-6 and a period-7 attractor. The basin of the period-6 point (left) occupies a smaller fraction of the* (x, y)*-plane than that of the period-7 point (right).*

Coexistence of a period-6 and a chaotic attractor. The parameter values $(\varphi_d, a) = (62.83, 3.468)$ lie in a region of the parameter plane where

a narrow "horn" with chaotic dynamics overlaps with the 1:6 tongue, see Figure 2.5. A stable period-6 point $(-0.370, 0.265)$ having complex Floquet multipliers $-0.53 \pm 0.77i$ is detected, and its basin (left panel of Figure 2.8) does not completely fill the region of no escape. With the initial condition $(0.193, 0.066)$ and 1000 transient iterations we also detect a strange attractor (right panel of Figure 2.8). Hence, a stable period-6 point and a chaotic attractor coexist for these parameter values.

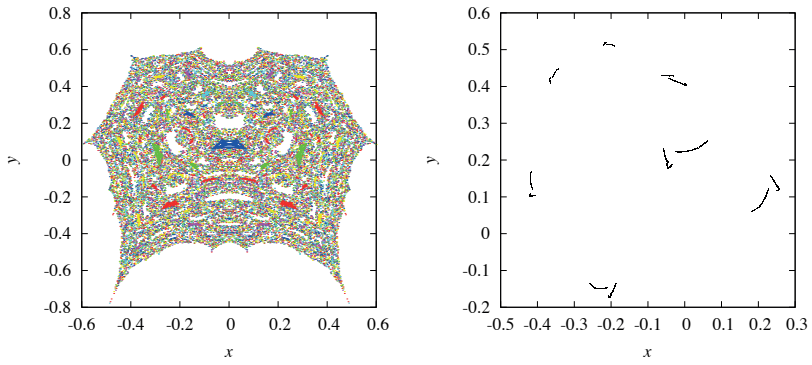

Figure 2.8. *For the parameter values* $(\varphi_d, a) = (62.83, 3.468)$ *a period-6 attractor coexists with a chaotic attractor. Left panel: the basin of attractor of the period-6 attractor. Right panel: the chaotic attractor.*

2.3.2 Chaotic dynamics and Hénon-like attractors

Figure 2.1 suggests that chaotic attractors with one positive or two positive Lyapunov exponents occur for regions in (φ, a)-plane having positive Lebesgue measure, and the question is how these attractors are formed. Moving parameters through a resonance tongue typically leads to a cascade of period doublings. We conjecture that strange attractors detected near the end of this cascade are Hénon-like, which means that they are equal to the closure of the unstable manifold of a saddle periodic point. Alternatively, a periodic point may first bifurcate via a secondary Hopf–Neĭmark–Sacker bifurcation leading to a new family of resonance tongues.

Near the 2:5 tongue. The parameter values $(\varphi_d, a) = (148, 3.3)$ belong to the 2:5 resonance tongue. When $\varphi_d = 148$ is kept constant and a is increased, a stable period-5 point bifurcates through a period doubling cascade into a strange attractor, see Figure 2.9. Observe that the second Lyapunov exponent becomes positive for $a \approx 3.5$. In the chaotic range one can observe periodic windows. In fact, they are conjectured to be dense, but this cannot be visualized with the finite resolution of the numerical computations.

Figures 2.10–2.12 show orbits of the map $\mathscr{T}$ and their power spectra for $\varphi_d = 148$ and three values of the parameter a. The power spectra show dominant peaks at the frequencies $f = 0.2$ and $f = 0.4$. These frequencies are inherited from the period-5 attractor having rotation number $\rho = 0.4$. As a increases the peak at $f = 0.2$ becomes weaker. In addition, broadband spectrum can be observed, which is typical for chaos.

At $a \approx 3.338$ a stable period-5 point loses stability through a period doubling bifurcation. The Lyapunov diagram in Figure 2.9 suggests that this is followed by an infinite cascade of period doublings. By numerical continuation we obtain a saddle period-5 point for the parameter values $a \in \{3.442, 3.48, 3.52\}$. Figures 2.10–2.12 show the unstable manifold computed for these saddle points. They have a remarkable resemblance to the orbits shown in the left panels. Hence, we conjecture that these attractors are in fact the closure of the unstable manifold of a saddle periodic point. This is akin to the classical Hénon map.

Strictly speaking, we must speak of an unstable set instead of an unstable manifold. Since the map $\mathscr{T}$ is not a diffeomorphism the unstable set can have self-intersections, and these can indeed be observed in Figures 2.10–2.12. The book by Mira et al. [44] describe possible mechanisms behind the formation of self-intersections of an unstable set of a saddle $Z_0 - Z_2$ maps. However, these results do not apply to $\mathscr{T}$ as we are now speaking of the unstable manifold of fixed points for $\mathscr{T}^5$ which is no longer of type $Z_0 - Z_2$.

Near the 1:5 tongue. Figure 2.13 shows a Lyapunov diagram for $\varphi_d = 72.5$ as a function of the parameter a. At $a \approx 3.416$ a stable period-5 point (having rotation number $\rho = 0.2$) loses stability through a period doubling bifurcation. Again an infinite cascade seems to take place afterwards. By numerical continuation we detect a saddle period-5 point for $a = 3.477$. The unstable manifold again is very similar to the strange attractor, see Figure 2.14.

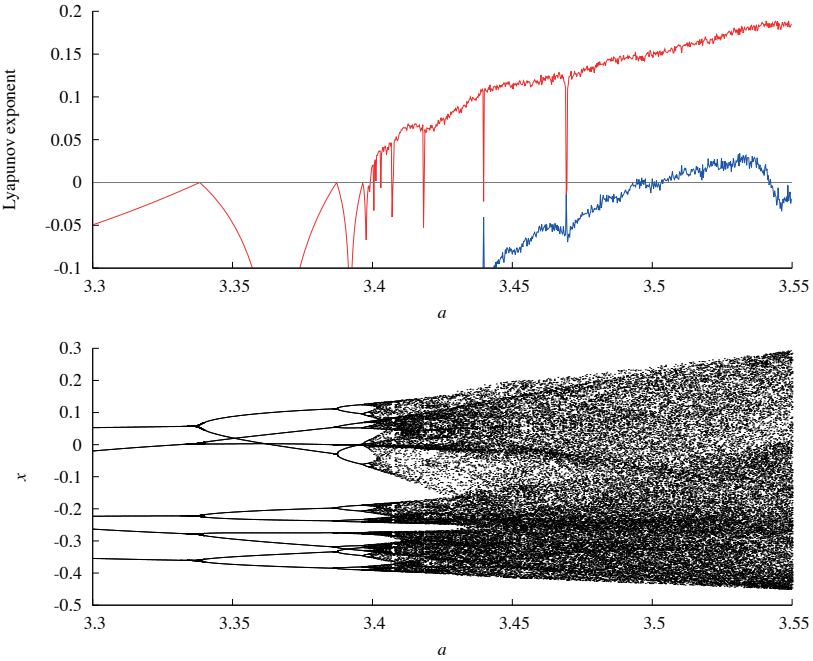

Figure 2.9. *Bifurcation diagram for $\varphi_d = 148$ and varying a. Top: Lyapunov exponents; a grey line indicating a zero LE has been added for clarity. Bottom: x-coordinates of the attractor.*

Note that the periodic point in the 1:5 tongue can also have complex Floquet multipliers Hence, it can also bifurcate through a secondary Hopf–Neĭmark–Sacker bifurcation, which leads to a new family of resonance tongues. This indeed happens, as is illustrated in the Lyapunov diagram of Figure 2.15. Also near these new tongues period doubling bifurcations take place. Hence, we can expect Hénon-like strange attractors in those regions of the parameter plane.

Near the 1:4 tongue. At $(\varphi_d, a) = (91.5, 3.)$ a stable period-4 point loses stability through a period doubling bifurcation. Again a cascade follows (Lyapunov diagram not shown). For $a = 3.54$ a strange attractor is detected,

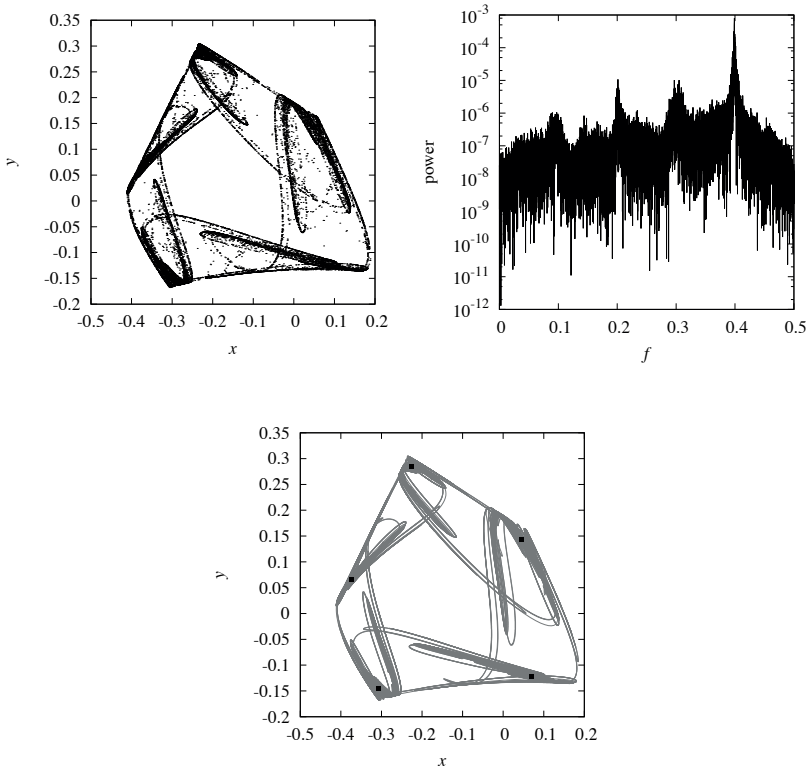

Figure 2.10. *An attractor detected for* $(\varphi_d, a) = (148, 3.442)$ *and its power spectrum. For these parameter values a period-5 point of saddle type exists and its unstable set shows a remarkable resemblance to the attractor.*

see Figure 2.16. This case is different from the previous ones: now it is *not* the period-4 point turning into a saddle. Indeed, the power spectrum of the attractor shows dominant peaks at the frequencies $f = 0.125$, $f = 0.25$, and $f = 0.375$. For the parameter value $a = 3.54$ no saddle period-4 point is detected. However, a saddle period-8 point does exist, and its unstable manifold resembles the attractor.

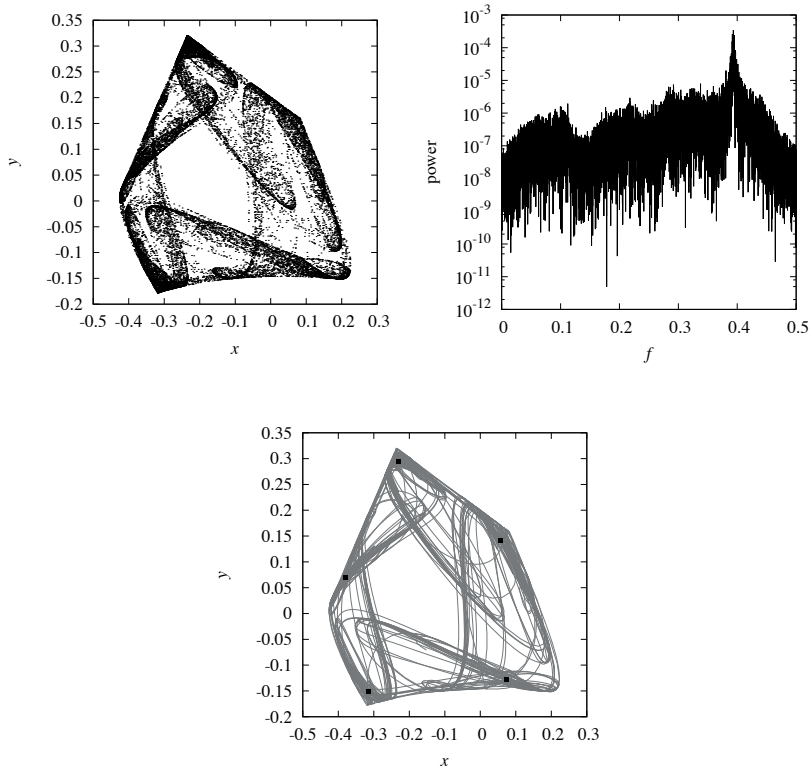

Figure 2.11. *As Figure 2.10, but for* $(\varphi_d, a) = (148, 3.48)$.

For $\varphi_d = 90$ the map $\mathscr{T}_{\varphi,a}$ is given by

$$\mathscr{T}_{\varphi,a}(x,y) = \begin{pmatrix} -y \\ f(x) \end{pmatrix} \quad \Rightarrow \quad \mathscr{T}^2_{\varphi,a}(x,y) = \begin{pmatrix} -f(x) \\ f(y) \end{pmatrix},$$

so that $\mathscr{T}^2$ just gives the iterates of the quadratic map f in both the x- and y-directions. For a sufficiently large the quadratic map has a chaotic orbit, and this leads, again via a period doubling cascade, to chaotic sets with two positive Lyapunov exponents. Some examples are shown in Figure 2.17.

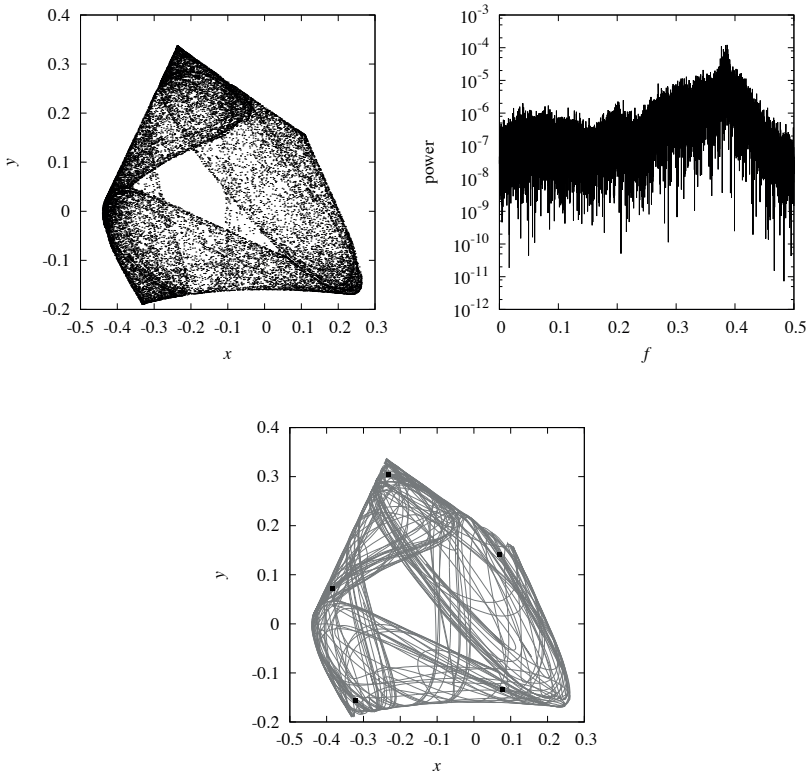

Figure 2.12. *As Figure 2.10, but for* $(\varphi_d, a) = (148, 3.52)$.

2.4 Discussion

In this Chapter we have studied the dynamics of a planar endomorphism which is composed of a fold and a rigid rotation.

We have proven analytically the existence of a Hopf–Neĭmark–Sacker bifurcation, which gives rise to Arnold tongues in the parameter plane of the map. Inside an Arnold tongue a periodic attractor typically either undergoes a period doubling cascade, which leads to chaotic dynamics, or a another

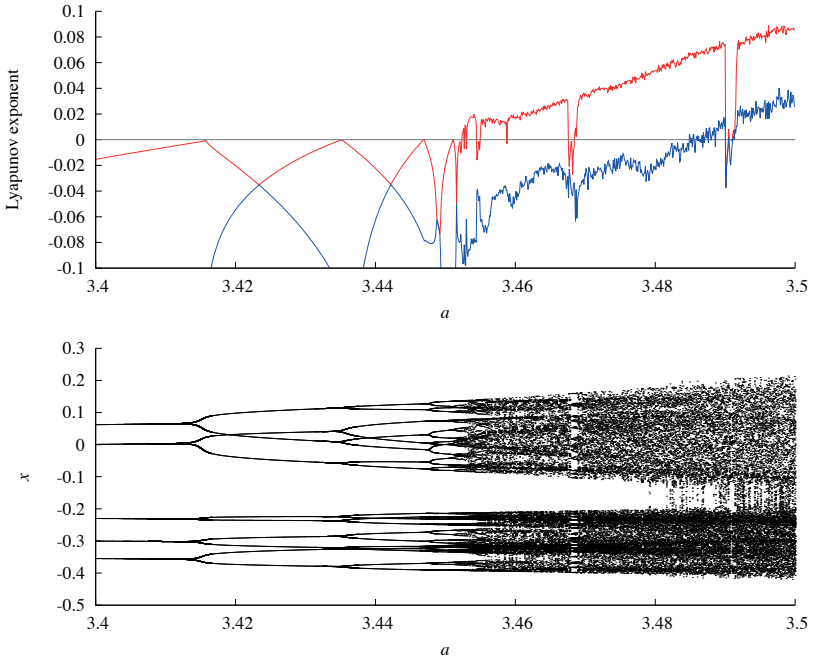

Figure 2.13. *Bifurcation diagram for $\varphi_d = 72.5$ and varying a. Top: Lyapunov exponents; a grey line indicating a zero LE has been added for clarity. Bottom: x-coordinates of the attractor.*

Hopf–Neĭmark–Sacker bifurcation, which in turn leads to a new family of Arnold tongues.

Our numerical experiments suggest that the map $\mathscr{T}_{\varphi,a}$ has attractors of Hénon-like type, i.e., attractors formed by the closure of an unstable set of a periodic point of saddle type. The Lyapunov diagram of Figure 2.1 suggests that these attractors occur within sets of positive measure in the (φ, a)-plane. However, a fundamental difference with Hénon-like observed in diffeomorphisms is that the attractors in this Chapter have a folded structure which is caused by the existence of (the iterates) of the critical line which divides the plane in regions for which the map $\mathscr{T}_{\varphi,a}$ has a different number of preimages. In particular, the unstable set of a saddle periodic point can

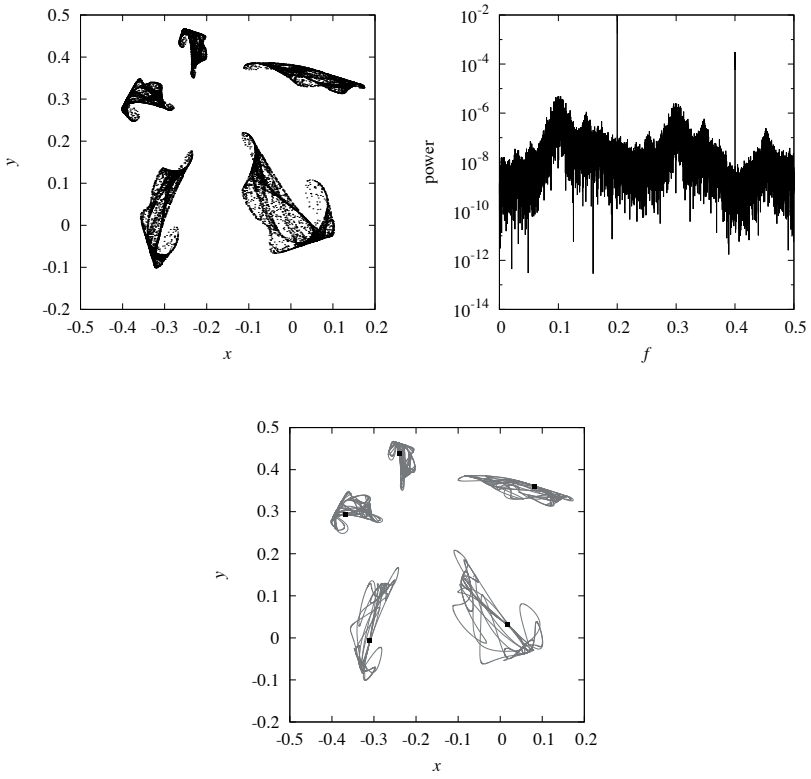

Figure 2.14. *As Figure 2.10, but for* $(\varphi_d, a) = (72.5, 3.477)$.

have self-intersections, which is not possible in diffeomorphisms.

An open question, which warrants further research, is whether the existence of Hénon-like strange attractors in endomorphisms can be rigorously proved. The current literature does provide existence proofs for some classes of diffeomorphisms, and essentially they are all obtained by perturbations of 1-dimensional maps [21, 45, 54]. Adapting the arguments to the setting of the map $\mathscr{T}$ could be a direction for future research. Apart from the existence question it is also important to investigate the prevalence of such attractors

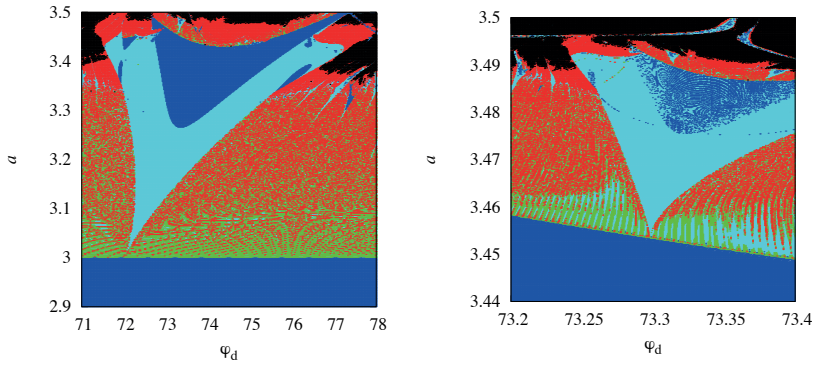

Figure 2.15. *Top: magnification of Lyapunov diagram in Figure 2.1 near the* $1:5$ *resonance tongue. Bottom: magnification of the top panel. See Table 2.1 for the colour coding.*

in parameter space.

Another open question is what bifurcation sequences lead to the formation of chaotic sets with two positive Lyapunov exponents and how they can be characterized geometrically. Numerical evidence suggests that these attractors occur within sets of positive measure in the parameter plane. For $\varphi = \pi/2$ the second iterate of the map $\mathcal{T}_{\varphi,a}$ is just given by decoupled iterates of the logistic map in the x and y components, which implies that the attractor is simply the Cartesian product of two cantor sets. However, for $\varphi \neq \pi/2$ the structure might be different.

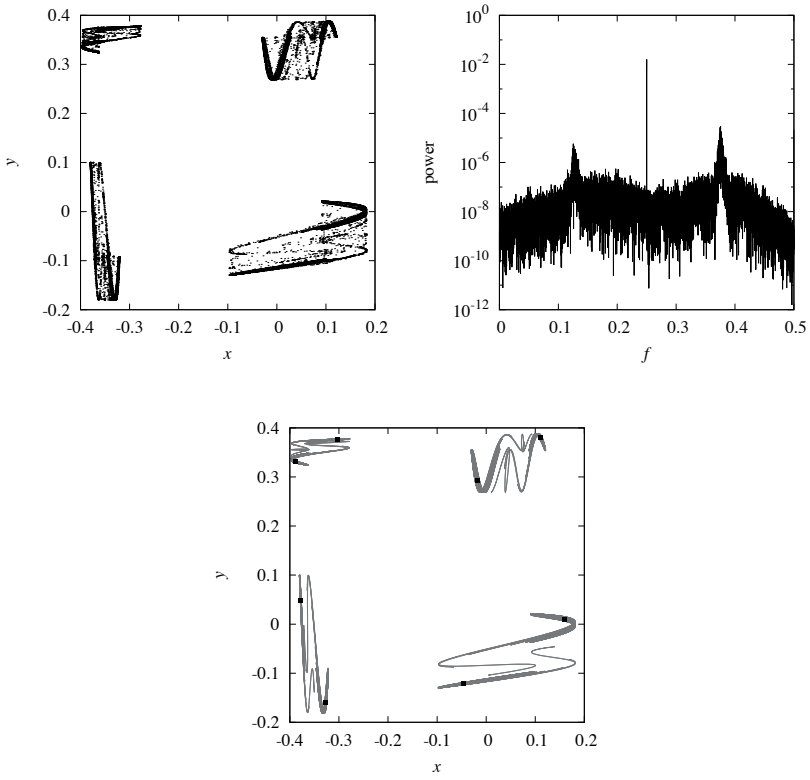

Figure 2.16. *As Figure 2.10, but for* $(\varphi_d, a) = (91.5, 3.54)$.

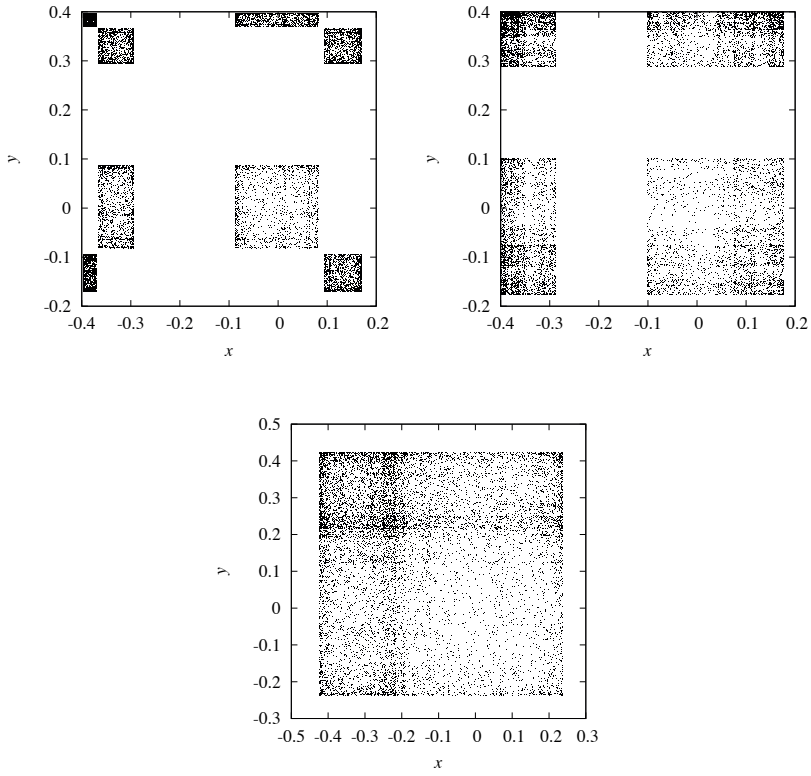

Figure 2.17. *Chaotic sets with two positive Lyapunov exponents for* $\varphi_d = 90$.

Chapter 3

Dynamics near folding and twisting

3.1 Introduction

In this Chapter we compare the dynamics of three planar, non-invertible maps which all rotate and fold the plane. Two of these maps are related to phenomena in biology and physics, whereas the the third map is *constructed* to serve as a toy model for the other two maps.

A predator-prey model. Consider the following planar map

$$\mathscr{P} : \begin{pmatrix} x \\ y \end{pmatrix} \mapsto \begin{pmatrix} ax(1-x-y) \\ bxy \end{pmatrix}. \tag{3.1}$$

This map is a simplification of the predator-prey model studied in [6]; also see [44] and references therein. In this Chapter we restrict to the parameter range $1 < a < 5$ and $b > 5/2$.

The map $\mathscr{P}$ is not invertible. Indeed, in the region defined by $ab - 4bx - 4ay > 0$ the map $\mathscr{P}$ has two preimages. Moreover, this map has a fixed point $(\frac{1}{b}, 1 - \frac{1}{a} - \frac{1}{b})$, which has complex eigenvalues for the parameters $b > (a + \sqrt{a})/(2a - 2)$. Hence, the map $\mathscr{P}$ rotates points near this fixed point.

A discretized Lorenz-63 model. Our second example arises from the classical Lorenz-63 model [37, 38] for Rayleigh-Bénard convection:

$$\frac{dx}{dt} = -\sigma(x-y), \qquad \frac{dy}{dt} = \rho x - y - xz, \qquad \frac{dz}{dt} = -\beta z + xy.$$

Taking the limit $\sigma \to \infty$ and replacing x with y gives a system of two differential equations:

$$\frac{dy}{dt} = (\rho - 1)y - yz, \qquad \frac{dz}{dt} = -\beta z + y^2.$$

In what follows, we will relabel the variables (y, z) as (x, y) again. In this 2-dimensional system we can assume without loss of generality that $\beta = 1$ by a suitable rescaling (but note that this property does not hold for the 3-dimensional system). After discretizing these equations by means of a forward Euler scheme with time step τ we obtain the map

$$\mathscr{L} : \begin{pmatrix} x \\ y \end{pmatrix} \mapsto \begin{pmatrix} (1+\alpha\tau)x - \tau xy \\ (1-\tau)y + \tau x^2 \end{pmatrix}, \tag{3.2}$$

where $\alpha = \rho - 1$. In this Chapter, we restrict to the parameter range $0 < \alpha < 1$ and $0 < \tau < 4$.

First note, that the map $\mathscr{L}$ is noninvertible. The curve defined by the equation

$$4\tau(y - cb)^3 = 27c^2x^2, \quad c = 1 - \tau, \quad b = (1 + \alpha\tau)/\tau,$$

separates two regions in the plane in which the map has either one or three preimages. In addition, the map has a fixed point $(\pm\sqrt{\alpha}, \alpha)$ of which the eigenvalues are complex for $\alpha > \frac{1}{8}$, see Proposition 6.

The fold-and-twist map. The maps $\mathscr{P}$ and $\mathscr{L}$ rotate points and fold the plane. Our aim is to study the combination of these effects in a map that is as simple as possible. To that end, we first define the map

$$\mathscr{F} : \begin{pmatrix} x \\ y \end{pmatrix} \mapsto \begin{pmatrix} f(x) \\ y \end{pmatrix},$$

where $f : \mathbb{R} \to \mathbb{R}$ is a continuous two-to-one map. Observe that $\mathscr{F}$ maps vertical lines onto vertical lines. In the following we will take

$$f(x) = \tfrac{1}{4}(a-2) - ax^2$$

which is conjugate to the logistic family $g(x) = ax(1-x)$. Indeed, for $\psi(x) = x - \frac{1}{2}$ we have that $f \circ \psi = \psi \circ g$. Hence, we will restrict to the parameter range $a \in [0, 4]$. Next, we consider a rigid rotation around the origin given by

$$\mathscr{R} : \begin{pmatrix} x \\ y \end{pmatrix} \mapsto \begin{pmatrix} x\cos\varphi - y\sin\varphi \\ x\sin\varphi + y\cos\varphi \end{pmatrix}.$$

The "fold-and-twist map" $\mathscr{T}$ is defined as the composition

$$\mathscr{T} = \mathscr{R} \circ \mathscr{F} : \begin{pmatrix} x \\ y \end{pmatrix} \mapsto \begin{pmatrix} f(x)\cos\varphi - y\sin\varphi \\ f(x)\sin\varphi + y\cos\varphi \end{pmatrix}. \tag{3.3}$$

The angle φ is measured in radians. However, for numerically obtained results values are reported in degrees, which is indicated by means of a subscript: $\varphi_d = 180\varphi/\pi$. It is easy to verify that the maps $\mathscr{T}_{\varphi,a}$ and $\mathscr{T}_{2\pi-\varphi,a}$ are conjugate via $\Psi(x, y) = (x, -y)$. In particular, the bifurcation diagram in the (φ, a)-plane is symmetric with respect to the line $\varphi = \pi$. Therefore, it suffices to study the family $\mathscr{T}_{\varphi,a}$ for $0 \le \varphi \le \pi$.

The dynamical properties of the map $\mathscr{T}$ were explored in [26]. The advantage of the map $\mathscr{T}$ is that the folding and twisting can be controlled separately using the parameters a and φ, and the idea of this Chapter is that the map $\mathscr{T}$ may serve as a "guide" to study and explain phenomena in the maps $\mathscr{P}$ and $\mathscr{L}$.

3.2 Overview of the dynamics

The Lyapunov diagrams in Figures 3.1–3.3 show a classification of the dynamical behavior of the maps $\mathscr{P}$, $\mathscr{L}$, and $\mathscr{T}$ in different regions of their parameter planes. See Appendix B.1 for a description of the algorithm used to compute Lyapunov exponents. Note that the three diagrams have a very similar geometric organization. In particular, one can observe a prevalence of periodic dynamics and chaotic dynamics. In all three diagrams one can observe tongue-shaped regions emanating along a curve. This suggests the presence of a Hopf–Neĭmark–Sacker bifurcation. Propositions 5–7 in Section 3.3.1 confirm that this is indeed the case.

The Lyapunov diagrams also suggest that chaotic attractors with one or two positive Lyapunov exponents occur for regions in the parameter plane with positive Lebesgue measure, and the question is how these attractors are formed and what their geometric structure is. Numerical evidence suggest

Color	Lyapunov exponents	Attractor type
cyan	$0 > \lambda_1 > \lambda_2$	periodic point of node type
blue	$0 > \lambda_1 = \lambda_2$	periodic point of focus type
green	$0 = \lambda_1 > \lambda_2$	invariant circle
red	$\lambda_1 > 0 \geq \lambda_2$	chaotic attractor
black	$\lambda_1 \geq \lambda_2 > 0$	chaotic attractor
white		no attractor detected

Table 3.1. *Color coding for the Lyapunov diagram of Figures 3.1, 3.2, and 3.3. The diagrams suggest that periodic attractors and chaotic attractors with 1 or 2 positive Lyapunov exponents occur for regions in the parameter plane with positive Lebesgue measure.*

that strange attractors having one positive Lyapunov exponent are of Hénon-like type, i.e., they are formed by the closure of the unstable manifold of a periodic point of saddle type. However, unlike in diffeomorphisms, these attractors have a folded structure in our maps.

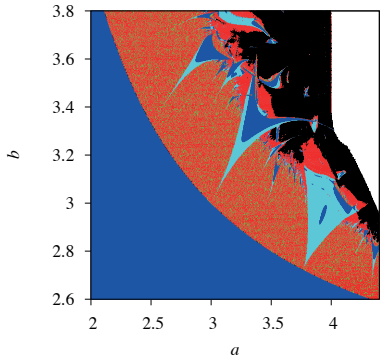

Figure 3.1. *Lyapunov diagram of attractors for the map $\mathscr{P}$ as a function of the parameters a and b. For the color coding see Table 3.1.*

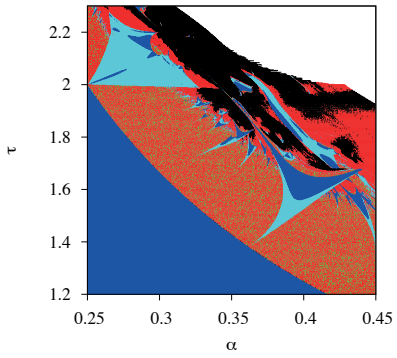

Figure 3.2. *As Figure 3.1, but for the map $\mathscr{L}$.*

3.3 Twisting and (quasi-)periodic dynamics

In this section we discuss periodic and quasi-periodic dynamics of the maps $\mathscr{P}$, $\mathscr{L}$, and $\mathscr{T}$. The Lyapunov diagrams already indicate that these type of dynamics occur in large regions of the parameter plane.

3.3.1 The Hopf-Neĭmark-Sacker bifurcation

The following three results confirm what is already suggested by the Lyapunov diagrams of Figures 3.1–3.3: along a curve in the parameter plane a stable fixed point bifurcates through a Hopf-Neĭmark-Sacker (HNS) bifurcation.

Proposition 5 (HNS bifurcation of the predator-prey map)**.** *The predator-prey map $\mathscr{P}$ has a fixed point $(\frac{1}{b}, 1-\frac{1}{a}-\frac{1}{b})$ which is stable if and only if*

$$1 < a < 9 \quad \textit{and} \quad \max\left\{\frac{a}{a-1}, \frac{3a}{a+3}\right\} < b < \frac{2a}{a-1}.$$

Along the curve $b = 2a/(a-1)$ the fixed point loses stability through a supercritical HNS bifurcation and gives birth to a unique stable, closed invariant circle. The strong resonances are located at the values $a \in \{1, 5, 7, 9\}$.

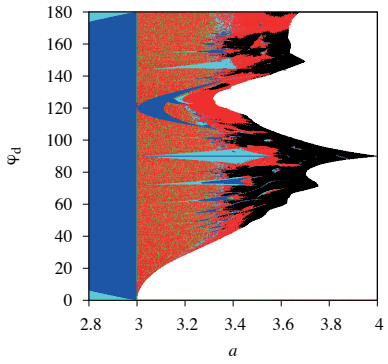

Figure 3.3. *As Figure 3.1, but for the map $\mathscr{T}$.*

Proof. Evaluating the Jacobian matrix of the map $\mathscr{P}$ at the fixed point $(\frac{1}{b}, 1 - \frac{1}{a} - \frac{1}{b})$ gives

$$J = \begin{pmatrix} 1 - a/b & -a/b \\ b - b/a - 1 & 1 \end{pmatrix},$$

which implies that $\det(J) = a - 2a/b$ and $\mathrm{tr}(J) = 2 - a/b$. From equation (A.1) it follows that the fixed point is stable if and only if the inequalities

$$1 < a < 9 \quad \text{and} \quad \max\left\{\frac{a}{a-1}, \frac{3a}{a+3}\right\} < b < \frac{2a}{a-1}$$

are satisfied. Along the curve $b = 2a/(a-1)$ the fixed point loses stability as a complex conjugate pair of eigenvalues crosses the unit circle with nonzero speed. At the HNS bifurcation the eigenvalues are given by

$$\lambda_\pm = \frac{5 - a \pm i\sqrt{16 - (5-a)^2}}{4} = e^{\pm i\theta} \quad \text{where} \quad \tan\theta = \frac{\sqrt{16 - (5-a)^2}}{5 - a}. \tag{3.4}$$

Strong resonances occur when $\lambda_\pm = 1$ (1:1 resonance), $\lambda_\pm = -1$ (1:2 resonance), $\lambda_\pm = -\frac{1}{2} \pm \frac{1}{2}\sqrt{3}i$ (1:3 resonance), and $\lambda = \pm i$ (1:4 resonance). From equation (3.4) it follows that these values of $\lambda_\pm$ are attained at $a = 1$, $a = 9$, $a = 7$ and $a = 5$, respectively.

We use equation (A.5) with $a_{22} = 1$, $a_{21} = 1$, and $a_{12} = (1-a)/2$. Computations with the computer algebra package Mathematica [58] then gives the following normal form coefficients:

$$h_{20} = \frac{-4a + 8ae^{i\theta} - 8ae^{2i\theta} + 4ae^{3i\theta}}{-3 + a + 4e^{i\theta} - 2e^{2i\theta}},$$

$$h_{11} = \frac{-4a + 10ae^{i\theta} - 8ae^{2i\theta} + 2ae^{3i\theta}}{(3-a)e^{i\theta} - 4e^{2i\theta} + 2e^{3i\theta}},$$

$$h_{02} = \frac{8a - 12ae^{-i\theta} + 4ae^{-2i\theta}}{3 - a - 4e^{i\theta} + 2e^{2i\theta}},$$

$$h_{21} = 0.$$

The expression of the first Lyapunov coefficient is rather complicated and will therefore be omitted. Figure 3.4 shows a graph of ℓ_1 as a function of the parameter a. Indeed, $\ell_1 < 0$ for $1 < a < 9$. This completes the proof. □

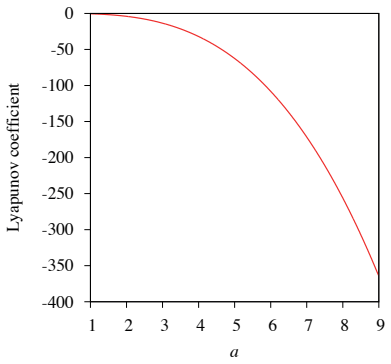

Figure 3.4. *Lyapunov coefficient as a function of the parameter a for the HNS bifurcation of the map $\mathscr{P}$.*

Proposition 6 (HNS bifurcation of the Lorenz map)**.** *The Lorenz map $\mathscr{L}$ has two fixed points $(\pm\sqrt{\alpha}, \alpha)$ which are stable when*

$$\alpha > 0 \quad \textit{and} \quad 0 < \tau < \min\left\{\frac{1-\sqrt{1-8\alpha}}{2\alpha}, \frac{1}{2\alpha}\right\}.$$

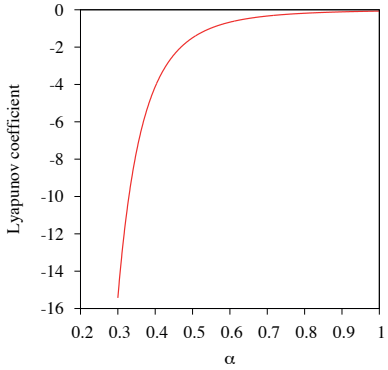

Figure 3.5. *Lyapunov coefficient as a function of the parameter α for the HNS bifurcation of the map $\mathscr{L}$.*

Along the curve $\tau = 1/2\alpha$ both fixed points lose stability through a supercritical HNS bifurcation which gives birth to a pair *of coexisting stable invariant circles. The strong resonances are located at the values $\alpha \in \{\frac{1}{4}, \frac{1}{6}, \frac{1}{8}\}$.*

Proof. Evaluating the Jacobian matrix of the map $\mathscr{L}$ at the fixed points $(\pm\sqrt{\alpha}, \alpha)$ is given by

$$J = \begin{pmatrix} 1 & \mp\tau\sqrt{\alpha} \\ \pm 2\tau\sqrt{\alpha} & 1-\tau \end{pmatrix},$$

which implies that $\det(J) = 1 - \tau + 2\alpha\tau^2$ and $\mathrm{tr}(J) = 2 - \tau$. From equation (A.1) it follows that a sufficient condition for stability of the fixed points is given by

$$\alpha > 0 \quad \text{and} \quad 0 < \tau < \min\left\{\frac{1-\sqrt{1-8\alpha}}{2\alpha}, \frac{1}{2\alpha}\right\}.$$

Along the curve $\tau = (1 - \sqrt{1-8\alpha})/2\alpha$ the fixed points lose stability as one eigenvalue passes -1. The eigenvalues become complex along the line $\alpha = \frac{1}{8}$. Along the curve $\tau = 1/2\alpha$, where $\alpha > \frac{1}{8}$, the fixed points lose stability through a complex conjugate pair of eigenvalues crossing the unit circle with nonzero speed. At the HNS bifurcation the eigenvalues are given by

$$\lambda_\pm = \frac{4\alpha - 1 \pm i\sqrt{8\alpha - 1}}{4\alpha} = e^{\pm i\theta} \quad \text{where} \quad \tan\theta = \frac{\sqrt{8\alpha-1}}{4\alpha - 1}. \tag{3.5}$$

Strong resonances occur when eigenvalues $\lambda_\pm = 1$ (1:1 resonance), $\lambda_\pm = -1$ (1:2 resonance), $\lambda_\pm = -\frac{1}{2} \pm \frac{1}{2}\sqrt{3}i$ (1:3 resonance), and $\lambda = \pm i$ (1:4 resonance). From equation (3.5) it follows that the 1:1 resonance does not occur. The remaning strong resonances occur for the values $\alpha = \frac{1}{8}$, $\alpha = \frac{1}{6}$, and $\alpha = \frac{1}{4}$, respectively.

We use equation (A.4) with $a_{11} = 1$, $a_{12} = -1/2\sqrt{\alpha}$, and $a_{21} = 1/\sqrt{\alpha}$. Computations with the computer algebra package Mathematica then gives the following normal form coefficients:

$$h_{20} = \frac{-3 + 3e^{i\theta}}{-2\alpha + 4\alpha^2 - 8\alpha^2 e^{i\theta} + 4\alpha^2 e^{2i\theta}},$$

$$h_{11} = \frac{-3 + e^{-i\theta} + 2e^{i\theta}}{-2\alpha + 4\alpha^2 - 8\alpha^2 e^{i\theta} + 4\alpha^2 e^{2i\theta}},$$

$$h_{02} = \frac{-3 + 2e^{-i\theta} + e^{i\theta}}{-2\alpha + 4\alpha^2 - 8\alpha^2 e^{i\theta} + 4\alpha^2 e^{2i\theta}},$$

$$h_{21} = 0.$$

The expression of the first Lyapunov coefficient is rather complicated and will therefore be omitted. Figure 3.5 shows a graph of ℓ_1 as a function of the parameter α. Indeed, $\ell_1 < 0$ for $\frac{1}{8} < \alpha$. This completes the proof. □

Proposition 7 (HNS bifurcation of the fold-and-twist map)**.** *For $0 < \varphi < 2\pi$ the map $\mathscr{T}$ has a fixed point $(\frac{2-a}{2a}, -\frac{2-a}{2a}\cot\frac{1}{2}\varphi)$ which loses stability through a supercritical HNS bifurcation along the line $a = 3$ and gives birth to a unique stable, closed invariant circle. The strong resonances are located at the values $\varphi \in \{\pi/2, 2\pi/3, \pi\}$.*

Proof. Evaluating the Jacobian matrix of the map $\mathscr{T}$ at the fixed point $(\frac{2-a}{2a}, -\frac{2-a}{2a}\cot\frac{1}{2}\varphi)$ gives the matrix

$$J = \begin{pmatrix} (a-2)\cos\varphi & -\sin\varphi \\ (a-2)\sin\varphi & \cos\varphi \end{pmatrix},$$

which implies that $\det(J) = a - 2$ and $\mathrm{tr}(J) = (a-1)\cos\varphi$. From equation (A.1) it follows that the fixed point is stable if and only if $1 < a < 3$. Along the line $a = 3$ the fixed point loses stability as a complex conjugate pair of eigenvalues crosses the unit circle with nonzero speed. At the HNS bifurcation the eigenvalues are simply given by $\lambda_\pm = e^{\pm i\varphi}$. It immediately follows that the strong resonances occur for $\varphi \in \{\pi/2, 2\pi/3, \pi\}$.

We use equation (A.4) with $a_{11} = \cos\varphi$, $a_{12} = -\sin\varphi$, and $a_{21} = \sin\varphi$. Computations with the computer algebra package Mathematica then gives the following normal form coefficients:

$$h_{20} = 3e^{i\varphi}\sin\varphi, \quad h_{11} = 3e^{i\varphi}\sin\varphi, \quad h_{02} = 3e^{i\varphi}\sin\varphi, \quad h_{21} = 0,$$

so that the first Lyapunov coefficient is given by

$$\ell_1 = -\frac{27}{2}\sin^2\varphi.$$

Clearly, $\ell_1 < 0$ for $0 < \varphi < \pi$. This completes the proof. □

Along each HNS bifurcation curve the eigenvalues of a fixed point are of the form $e^{\pm i\theta}$. At points where $\theta = p/q$ is rational so-called resonance tongues of order p:q emanate. These are indeed clearly visible in the Lyapunov diagrams of Figures 3.1–3.3. The boundaries of these tongues are formed by two saddle-node bifurcations, and for parameter values within a tongue a stable periodic point coexists with a saddle periodic point. The unstable manifold of the saddle periodic point forms an invariant circle. For the 1:5 resonance tongue of the map $\mathscr{P}$ such an invariant circle is shown in Figure 3.6. The invariant circles of the maps $\mathscr{L}$ and $\mathscr{T}$ are qualitatively similar and hence not shown. The points along the bifurcation curve for which $\theta \in \{2\pi, \pi, 2\pi/3, \pi/2\}$ are so-called strong resonances. For such parameter values more than one closed invariant curve can appear, or such a curve may not exist at all [34].

Upon parameter variation, the invariant circle can be destroyed by homoclinic tangencies between the stable and unstable manifolds of the unstable periodic point, or the circle can interact with other objects via heteroclinic tangencies. This scenario will not be considered in the present work, but see [11, 12] for an extensive discussion. Instead, we will focus on chaotic dynamics arising through bifurcations of the periodic points in the resonance tongues.

3.4 Folding and chaotic dynamics

In this section we discuss the implications of the non-invertible nature of the three maps. We will discuss Hénon-like attractors and their folded structure. In addition, we discuss the existence of snap-back repellers which is also a consequence of non-invertibility.

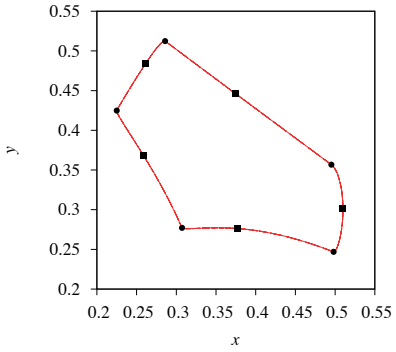

Figure 3.6. *Invariant circle in the 1:5 resonance tongue of the map $\mathscr{P}$ with $(a, b) = (3.9, 2.9)$ formed by the unstable manifolds of the saddle period-5 points (squares). The stable period-5 points are indicated by circles.*

3.4.1 Critical lines

An important tool in the study of non-invertible planar maps is the so-called critical manifold [43, 44]. For a smooth map $\mathscr{F} : \mathbb{R}^2 \to \mathbb{R}^2$ we define the set

$$LC_{-1} = \{(x, y) \in \mathbb{R}^2 \ : \ \det D\mathscr{F}(x, y) = 0\}.$$

The critical line LC (in French: "ligne critique") is then defined as the image of LC_{-1} under the map $\mathscr{F}$. The critical line LC and its iterates play an important role in the bifurcations of basin boundaries and in bounding invariant regions. The critical line for the maps studied in this work are given by the following propositions. These results follow in a straightforward manner from the definitions given above, and therefore their proofs are omitted.

Proposition 8 (Critical line of the predator-prey map)**.** *For the map $\mathscr{P}$ the critical line and its inverse image are given by the equations*

$$\begin{aligned} LC_{-1} &: \ x = \tfrac{1}{2}, \\ LC &: \ bx + ay = \tfrac{1}{4}ab. \end{aligned}$$

Proposition 9 (Critical line of the Lorenz map)**.** *For the map $\mathscr{L}$ with $\tau > 0$ and $\tau \neq 1$ the critical line and its inverse image are given by the equations*

$$\begin{aligned} LC_{-1} &: \; y = \frac{1+\alpha\tau}{\tau} + \frac{2\tau x^2}{1-\tau}, \\ LC &: \; \left(y - \frac{(1-\tau)(1+\alpha\tau)}{\tau} \right)^3 = \frac{27(1-\tau)^2 x^2}{4\tau}. \end{aligned}$$

If $\tau = 1$ then LC_{-1} is given by the line $x = 0$ so that LC reduces to the single point $(0, 0)$.

Proposition 10 (Critical line of the fold-and-twist map)**.** *For the map $\mathscr{T}$ the critical line and its inverse image are given by the equations*

$$\begin{aligned} LC_{-1} &: \; x = 0, \\ LC &: \; x\cos\varphi + y\sin\varphi = \tfrac{1}{4}(a-2). \end{aligned}$$

Now consider any smooth, noninvertible map $\mathscr{F} : \mathbb{R}^2 \to \mathbb{R}^2$. Under general conditions the set LC_{-1} is a smooth curve in $\mathbb{R}^2$. A sufficient condition for this is, for example, that 0 is a regular value of the map $(x, y) \mapsto \det D\mathscr{F}(x, y)$. This is indeed the case for the maps $\mathscr{P}$, $\mathscr{L}$, and $\mathscr{T}$. Assume that LC_{-1} is parameterized with $\lambda : I \to \mathbb{R}^2$, where I is an open interval around 0. Now let $\gamma : I \to \mathbb{R}^2$ be any other smooth curve that intersects the curve $LC_{-1} = \lambda$. Without loss of generality we may assume that $\gamma(0) = \lambda(0)$. The vectors $\gamma'(0)$ and $\lambda'(0)$ are the tangent vectors to the curves γ and λ at their point of intersection.

The image $\mathscr{F}(\lambda)$ is by definition the critical line LC. Note that the image $\mathscr{F}(\gamma)$ may have self-intersections due to the noninvertibility of $\mathscr{F}$. Away from such self-intersections $\mathscr{F}(\gamma)$ is again a smooth curve which intersects the critical line LC at the point $\mathscr{F}(\gamma(0)) = \mathscr{F}(\lambda(0))$. The tangent vectors at this point are given by $D\mathscr{F}(\gamma(0))\gamma'(0)$ and $D\mathscr{F}(\lambda(0))\lambda'(0)$. Since $\gamma(0) = \lambda(0) \in LC_{-1}$ it follows that the matrix $D\mathscr{F}(\gamma(0))$ has rank 1 which means that the vectors $D\mathscr{F}(\gamma(0))\gamma'(0)$ and $D\mathscr{F}(\lambda(0))\lambda'(0)$ are parallel. This implies that the curve $\mathscr{F}(\gamma)$ is *tangent* to LC at $\mathscr{F}(\gamma(0))$. An exception to this situation is when the vector $\gamma'(0)$ belongs to the null space of $D\mathscr{F}(\gamma(0))$ in which case $\mathscr{F}(\gamma)$ has a *cusp* point intersection with LC. These two cases are illustrated for the fold-and-twist map $\mathscr{T}$ with $(a, \varphi) = (3.2, 2\pi/5)$ in Figures 3.7 and 3.8.

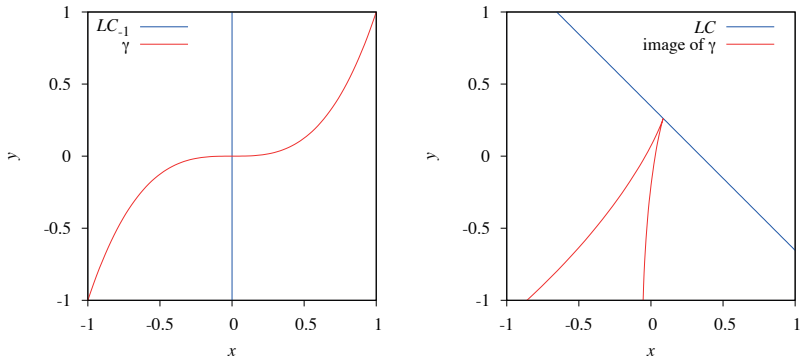

Figure 3.7. *The curve $\gamma(t) = (t, t^3)$ intersects the line LC_{-1}. Its image intersects the line LC in a cusp.*

3.4.2 Routes to chaos and Hénon-like attractors

In this section we investigate the routes to chaos and the structure of chaotic attractors for the three maps. The discussion will be restricted to resonance tongues of order 1:4, 1:5, and 2:5 since these tongues are the largest in the parameter plane in the sense of Lebesgue measure. Near other tongues we expect similar dynamical behavior.

Near a HNS bifurcation a resonance tongue contains a pair of stable and unstable periodic points. The stable periodic point is either a node (real eigenvalues) or a focus (complex eigenvalues). Periodic points of focus type typically bifurcate through a secondary HNS bifurcation, which leads to a new set of resonance tongues. The newly created periodic points in these secondary tongues can undergo period-doubling bifurcations or HNS bifurcations. For this reason we restrict the discussion to the primary resonance tongues in which the stable periodic point is a node.

The periodic points of node type typically undergo a period-doubling cascade upon parameter variation. This is illustrated by means of Lyapunov diagrams for the maps $\mathscr{P}$, $\mathscr{L}$, and $\mathscr{T}$ in Figures 3.9–3.11. Period doubling cascades lead to the creation of infinitely many unstable periodic points. These points play a key role in the formation of chaotic attractors in two different ways. One scenario is that a periodic point of source type becomes

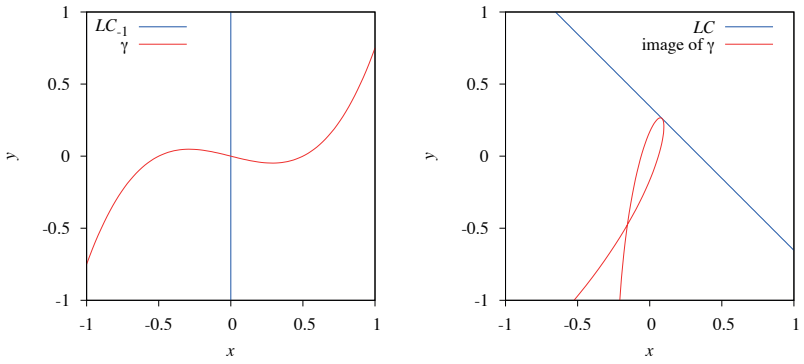

Figure 3.8. *The curve* $\gamma(t) = (t, t(t+\frac{1}{2})(t,(t-\frac{1}{2}))$ *intersects the line* LC_{-1}*. Its image is tangent to* LC*. Note that the image of* γ *also has a self-intersection.*

a so-called *snap-back repeller*, which provides a sufficient condition for chaotic dynamics. We will discuss snap-back repellers in more detail in Section 3.4.3.

Another scenario is that a periodic point of saddle type has an unstable manifold which shows a strong resemblance to the chaotic attractor observed for the same parameter values. Such attractors will be referred to as *Hénon-like* attractors. Numerical evidence of Hénon-like attractors for the maps $\mathscr{P}$ (in the 1:5 tongue), $\mathscr{L}$ (in the 1:4 tongue), and $\mathscr{T}$ (in the 2:5 tongue) is presented in Figures 3.12–3.14. Each figure shows a chaotic attractor together with the unstable manifold of a saddle periodic point. Due to the striking resemblance we conjecture that each chaotic attractor shown is in fact the closure of an unstable manifold of the saddle point.

Note that strictly speaking, we must speak of an "unstable set" instead of an "unstable manifold". Indeed, since the maps $\mathscr{P}$, $\mathscr{L}$, and $\mathscr{T}$ are not diffeomorphisms the unstable set can have self-intersections which are indeed clearly visible in the aforementioned figures. An explanation of this phenomenon is already provided in Section 3.4.1 where it is shown that the image of any curve under a noninvertible map may have self-intersections. Figure 3.15 shows a close up of the Hénon-like attractor of Figure 3.12 together with iterates of the critical line LC. Clearly, the unstable manifolds

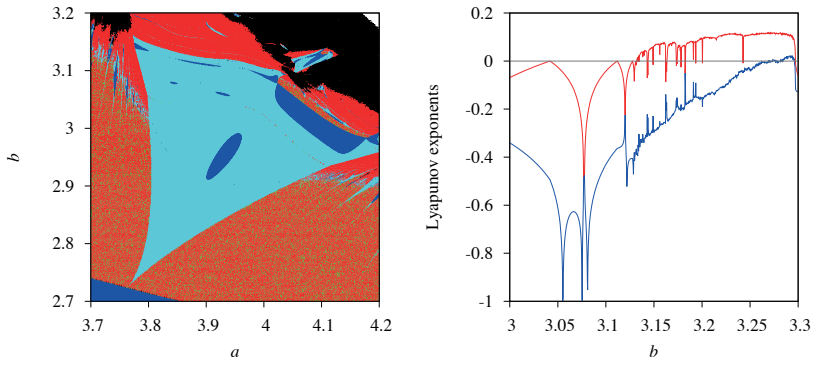

Figure 3.9. *Left panel: 1:5 resonance tongue of $\mathscr{P}$ in the (a, b)-plane. Right panel: Lyapunov exponents as a function of the parameter b while keeping the parameter $a = 3.85$ fixed.*

forms tangencies along the iterates of LC. Observe that LC is described by a linear equation and its iterate is an algebraic curve of degree 2. Therefore, the n-th iterate of LC is an algebraic curve of degree 2^n. Hence, iterates of LC become very complex and so do the foldings of the unstable manifolds.

3.4.3 Snap-back repellers

In his 1989 paper, in which the map $\mathscr{L}$ was introduced, Lorenz [38] pointed out the following sufficient condition for a non-invertible map to exhibit sensitive dependence on initial conditions: if the map has an attractor containing two distinct points which are mapped to the same point, then the map exhibits sensitive dependence on initial conditions. Lorenz only provided a heuristic argument and suggested that his observation is part of mathematical folklore. However, already in 1978 Marotto [39] proved a theorem in this spirit that provides a sufficient condition for chaotic dynamics of multidimensional maps. In what follows $\|\cdot\|$ denotes the standard Euclidean norm on $\mathbb{R}^n$ and $B_r(p) := \{x \in \mathbb{R}^n \,:\, \|x-p\| \leq r\}$ denotes a closed ball with radius r around the point p.

Definition 2 (Marotto [39, 41])**.** *Let $\mathscr{F} : \mathbb{R}^n \to \mathbb{R}^n$ be a differentiable map.*

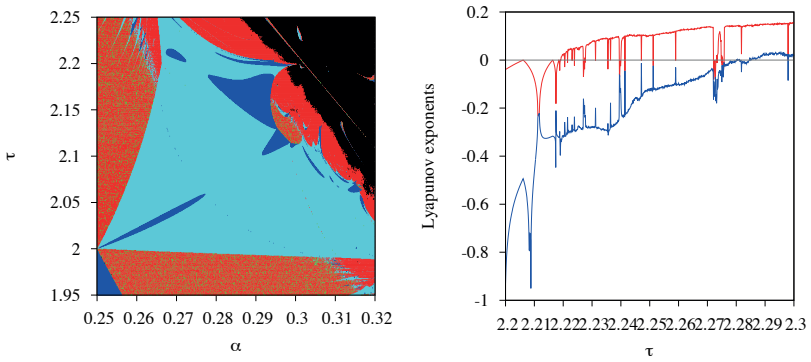

Figure 3.10. *As Figure 3.9, but for the 1:4 resonance tongue of the map $\mathscr{L}$. In the right panel the parameter $\alpha = 0.28$ is kept fixed.*

A fixed point p of $\mathscr{F}$ is called a snap-back repeller *if the following two conditions are satisfied:*

(i) the fixed point p is expanding*, which means that there exists an $r > 0$ such that the eigenvalues of $D\mathscr{F}(x)$ exceed 1 in absolute value for all $x \in B_r(p)$;*

(ii) there exists a point $x_0 \in B_r(p)$ with $x_0 \neq p$ and $m \in \mathbb{N}$ such that $x_m = p$ and $\det(D\mathscr{F}(x_k)) \neq 0$ for all $1 \leq k \leq m$ where $x_k = \mathscr{F}^k(x_0)$.

Theorem 1 (Marotto [39])**.** *If $\mathscr{F} : \mathbb{R}^n \to \mathbb{R}^n$ has a snap-back repeller, then $\mathscr{F}$ is chaotic in the sense of Marotto. That is, there exist*

(i) $N \in \mathbb{N}$ such that for each $p \geq N$ the map $\mathscr{F}$ has a periodic point of period p;

(ii) a scrambled set *for $\mathscr{F}$, i.e., an uncountable set S containing no periodic points such that*

(a) $\mathscr{F}(S) \subset S$,

(b) for every $x, y \in S$ with $x \neq y$ we have

$$\limsup_{k\to\infty} \|\mathscr{F}^k(x) - \mathscr{F}^k(y)\| > 0,$$

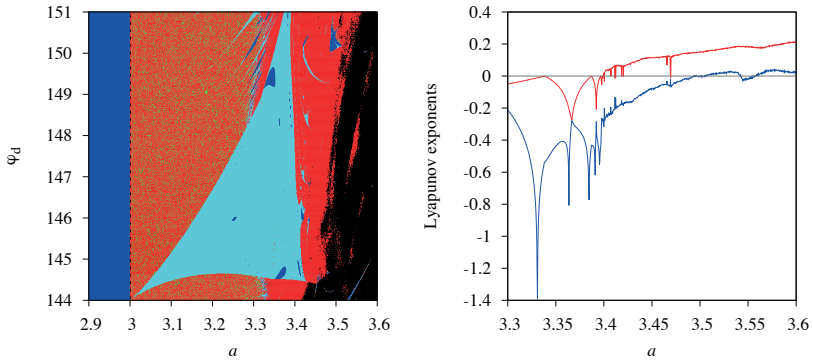

Figure 3.11. *As Figure 3.9, but for the 2:5 resonance tongue of the map $\mathscr{T}$. In the right panel the parameter $\varphi_d = 148$ is kept fixed.*

(c) for every $x \in S$ and any periodic point y we have

$$\limsup_{k\to\infty} \|\mathscr{F}^k(x) - \mathscr{F}^k(y)\| > 0,$$

(d) an uncountable subset S_0 of S such that for every $x, y \in S_0$ we have

$$\liminf_{k\to\infty} \|\mathscr{F}^k(x) - \mathscr{F}^k(y)\| = 0.$$

Of course, invertible maps cannot have snap-back repellers. For these maps the occurrence of chaotic dynamics is often proved via the existence of bifurcations that lead to homoclinic tangencies of stable and unstable manifolds of periodic points of saddle type, see Palis and Takens [46] for a general account. Marotto's theorem provides a sufficient condition for chaotic dynamics of non-invertible maps based on expanding periodic points and circumvents the computation of stable and unstable manifolds and their intersections. In this sense proving the occurrence of chaotic dynamics for noninvertible maps is easier than for invertible maps. Note that the existence of a snap-back repeller does not reveal the *structure* of a chaotic attractor. Below we will give numerical evidence of a snap-back repeller that coexists with a saddle periodic point giving rise to a Hénon-like attractor.

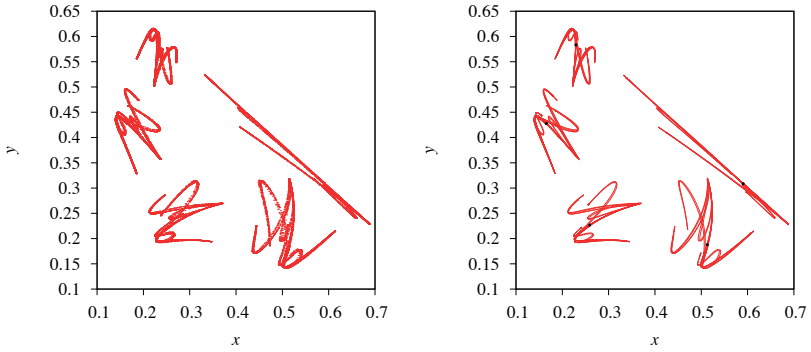

Figure 3.12. *A chaotic attractor of the map $\mathscr{P}$ for $(a, b) = (3.85, 3.2)$ (left panel) and the unstable manifold of a saddle period-5 point (right panel).*

The following theorem, of which the proof is based on the implicit function theorem, will be useful to prove the existence of snap-back repellers for a range of parameters of the fold-and-twist map $\mathscr{T}$.

Theorem 2 (Li & Lyu [35])**.** *Denote by $\|\cdot\|$ and $\|\cdot\|_{\text{op}}$ the Euclidean norm and the induced operator norm, respectively. Let $\mathscr{F} : \mathbb{R}^n \to \mathbb{R}^n$ be a C^1 map with a snap-back repeller. If $\mathscr{G} : \mathbb{R}^n \to \mathbb{R}^n$ is a C^1 map such that $\|\mathscr{F} - \mathscr{G}\| + \|D\mathscr{F} - D\mathscr{G}\|_{\text{op}}$ is sufficiently small, then $\mathscr{G}$ has a snap-back repeller.*

The concept of snap-back repellers is not new, but it is still the subject of intensive study. Some works that appeared in the last ten years are [19, 47, 48, 49, 50, 59, 60]. Note that differentiability of the map is an essential condition for Theorem 1, but see [24, 25] for results which do not require smoothness.

3.4.3.1 Existence of snap-back repellers for the map $\mathscr{T}$

In this section we prove the existence of snap-back repellers for the map $\mathscr{T}$ in the special case $\varphi = \pi/2$. First note that for this parameter value the periodic point born at the HNS bifurcation described in Proposition 7 can be computed explicitly.

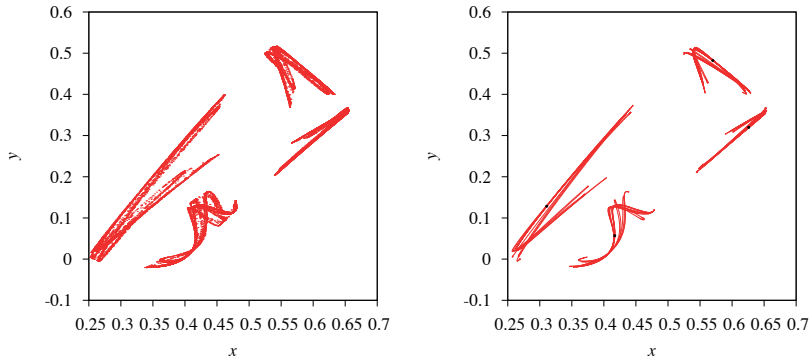

Figure 3.13. *As Figure 3.12, but for the map $\mathscr{L}$ with $(\alpha, \tau) = (0.28, 2.25)$.*

Proposition 11. *For $\varphi = \pi/2$ and $a > 3$ the fold-and-twist map $\mathscr{T}$ has three period-4 points which are given by $(-p_1, p_3)$, $(-p_2, p_3)$, and $(-p_4, p_4)$, where*

$$p_1 = -\frac{1}{2}, \quad p_2 = \frac{a-2}{2a}, \quad p_3 = \frac{1+\sqrt{(a-3)(a+1)}}{2a}, \quad p_4 = \frac{1-\sqrt{(a-3)(a+1)}}{2a}.$$

The points $(-p_1, p_3)$ and $(-p_2, p_3)$ are unstable. The point $(-p_4, p_4)$ is stable for $3 < a < 1+\sqrt{6}$, but loses stability at $a = 1+\sqrt{6}$ as two Floquet multipliers pass through -1. At $a = 3$ all three period-4 points coalesce with a fixed point.

Proof. Recall that $f(x) = \frac{1}{4}(a-2) - ax^2$. For $\varphi = \pi/2$ we have $\mathscr{T}(x, y) = (-y, f(x))$ so that $\mathscr{T}^4(x, y) = (-f^2(x), f^2(y))$. Hence, (x, y) is a period-4 point of $\mathscr{T}$ if and only if $-x$ and y are fixed points of f^2. For $3 < a < 4$ the fixed points for f^2 are given by $p_1, \ldots, p_4$. This implies that there are 16 candidates for a period-4 point of $\mathscr{T}$ which are given by $(-p_i, p_j)$ for $1 \le i, j \le 4$. Straightforward computations show that:

- $(-p_1, p_1)$ and $(-p_2, p_2)$ are unstable fixed points;
- $(-p_1, p_2) \mapsto (-p_2, p_1)$ is an unstable period-2 orbit;
- $(-p_1, p_3) \mapsto (-p_3, p_1) \mapsto (-p_1, p_4) \mapsto (-p_4, p_1)$ is a period-4 orbit;

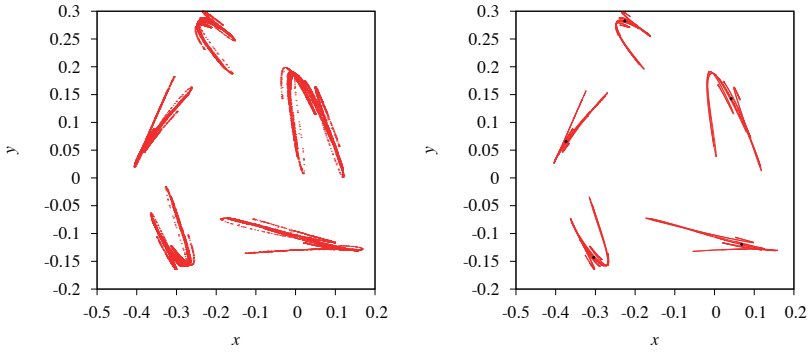

Figure 3.14. *As Figure 3.12, but for the map* $\mathscr{T}$ *with* $(a, \varphi_d) = (3.43, 148)$.

- $(-p_2, p_3) \mapsto (-p_3, p_2) \mapsto (-p_2, p_4) \mapsto (-p_4, p_2)$ is a period-4 orbit;
- $(-p_4, p_4) \mapsto (-p_4, p_3) \mapsto (-p_3, p_3) \mapsto (-p_3, p_4)$ is a period-4 orbit.

This exhausts all period-4 orbits. The Floquet multipliers of a period-4 point $(-p_i, p_j)$ are given by $\lambda_1 = 4a^2 p_i f(p_i)$ and $\lambda_2 = 4a^2 p_j f(p_j)$. This implies the following conclusions:

- $(-p_1, p_3)$ has Floquet multipliers $\lambda_1 = a^2$ and $\lambda_2 = 1 - (a-3)(a+1)$, and since $a > 3$ this point is unstable;
- $(-p_2, p_3)$ has Floquet multipliers $\lambda_1 = (2-a)^2$ and $\lambda_2 = 1-(a-3)(a+1)$, and since $a > 3$ this point is unstable;
- $(-p_4, p_4)$ has Floquet multipliers $\lambda_1 = \lambda_2 = 1 - (a-3)(a+1)$. Note that $|\lambda_{1,2}| < 1$ for $3 < a < 1 + \sqrt{6}$, and at $a = 1 + \sqrt{6}$ both multipliers pass through -1.

This completes the proof. □

We now prove that p_4 is a snap-back repeller for f^2 when $a = 4$. Next, we use this result to show that $(-p_4, p_4)$ is a snap-back repeller for $\mathscr{T}^4$.

Lemma 3. *For* $1+\sqrt{6} < a \leq 4$ *the point* $p = \left(1-\sqrt{(a+1)(a-3)}\right)/2a$ *is an expanding fixed point of the second iterate of the map* $f(x) = \frac{1}{4}(a-2) - ax^2$.

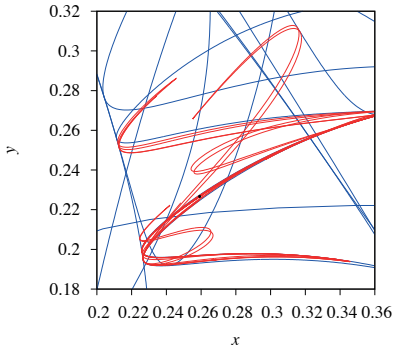

Figure 3.15. *Close up of the Hénon-like attractor of Figure 3.12 together with some iterates of the critical line LC (in blue).*

Proof. Let $g = f^2$, then $g(p) = p$. Note that $g'(x) = -4a^3x^3 + a^2(a-2)x$ has a local minimum at $m = -\sqrt{(a-2)/12a}$. It is straightforward to verify that $g'(m)$ is a decreasing function of a and that $g'(m) = -1$ for $a = 3$. Since $g'(-\frac{1}{2}) = a^2 > 0$ and $g'(0) = 0$ it follows from the intermediate value theorem that for $a > 3$ there exist numbers $-\frac{1}{2} < \xi < m < \eta < 0$ such that $g'(x) = -1$ for $x = \xi$ and $x = \eta$. Hence, $g'(x) < -1$ for all $x \in U := (\xi, \eta)$. For $a = 1 + \sqrt{6}$ we have that $p = \xi = (1 - \sqrt{2})/(2 + 2\sqrt{6})$ so that the point p lies on the boundary of U. For $1 + \sqrt{6} < a \leq 4$ the point p is contained in U. In this case the ball $B_r(p)$ with $r < \min\{|p - \xi|, |p - \eta|\}$ is a repelling neighborhood of p. □

Lemma 4. *For $a = 4$ the second iterate of the map $f(x) = \frac{1}{4}(a-2) - ax^2$ has a snap-back repeller.*

Proof. Let $a = 4$ and define $g(x) = f^2(x) = -\frac{1}{2} + 16x^2 - 64x^4$. Lemma 3 shows that $p = (1 - \sqrt{5})/8$ is an expanding fixed point of g. Hence, there exists $r > 0$ such that $|g'(x)| > 1$ for all $x \in B_r(p)$. Set $x_1 = -p$ so that $g(x_1) = p$. Consider the sequence $x_{k+1} = h(x_k)$ where

$$h(x) = -\tfrac{1}{4}\sqrt{2 - \sqrt{2 - 4x}}$$

is one of the four branches of the multi-valued inverse of g. Since h is strictly decreasing we have that $I := h([-\frac{1}{2}, \frac{1}{2}]) = [-\frac{1}{2\sqrt{2}}, 0]$. Note that h maps I into itself so that $x_k \in I$ for all $k \geq 2$. Since $|h'(x)| < 1$ for all $x \in I$ the mean value theorem shows that $h : I \to I$ is a contractive mapping. Since $p \in I$ is a fixed point of h it follows that $x_k \to p$ as $k \to \infty$. Hence, for $m \in \mathbb{N}$ sufficiently large we have $x_m \in B_r(p)$ and $g^m(x_m) = p$. First note that $g'(x_1) = g'(-p) = 4$, and then observe that for $k \geq 2$ the points x_k lie in the interior of the interval I and $g'(x)$ is only zero at the boundary points of I. Therefore, $g'(x_i) \neq 0$ for all $i = 1, \ldots, m$. □

Proposition 12. *Let $\epsilon > 0$ be sufficiently small. For $4 - \epsilon < a \leq 4$ and $\pi/2 - \epsilon < \varphi < \pi/2 + \epsilon$ the fourth iterate of the fold-and-twist map $\mathscr{T}$ has a snap-back repeller.*

Proof. Note that for $\varphi = \pi/2$ we have $\mathscr{T}(x, y) = (-y, f(x))$ so that $\mathscr{T}^4(x, y) = (-f^2(x), f^2(y))$. Lemma 4 shows that f^2 has a snap-back repeller p in some repelling neighbourhood $(p - r, p + r)$ for $a = 4$. It is straightforward to check that $(-p, p)$ in the neighbourhood $B_r((-p, p))$ is a snap-back repeller for $\mathscr{T}^4$ for $(a, \varphi) = (4, \pi/2)$. Applying the persistence result of Theorem 2 completes the proof. □

3.4.3.2 Numerical evidence of snap-back repellers

In theory the conditions for a snap-back repeller are easy to verify since the computation of invariant manifolds is circumvented. However, rigorous proofs for the existence of a snap-back repeller are only possible in cases for which the "return time" m in Definition 2 is relatively small. Indeed, if $\mathscr{F} : \mathbb{R}^d \to \mathbb{R}^d$ is a k-to-1 map, then the number of preimages of a fixed point under $\mathscr{F}^m$ is k^m. Therefore, the explicit computation of preimages is only possible for small values of m. In general, it can be expected that when the radius of the repelling neighborhood decreases, a larger number of preimages may be needed in order to return to the neighborhood of the periodic point. Figure 3.16 illustrates this phenomenon for the map $\mathscr{T}$.

The three maps $\mathscr{P}$, $\mathscr{L}$, and $\mathscr{T}$ all have a fixed point which becomes a source through the HNS bifurcation described in Section 3.3.1. The numerical evidence presented in Figures 3.17-3.19 suggests that for suitable choices of the parameter values the fixed point can become a snap-back repeller. For the three maps we have numerically computed a sequence of preimages by recursively applying the formulas for the inverses presented in

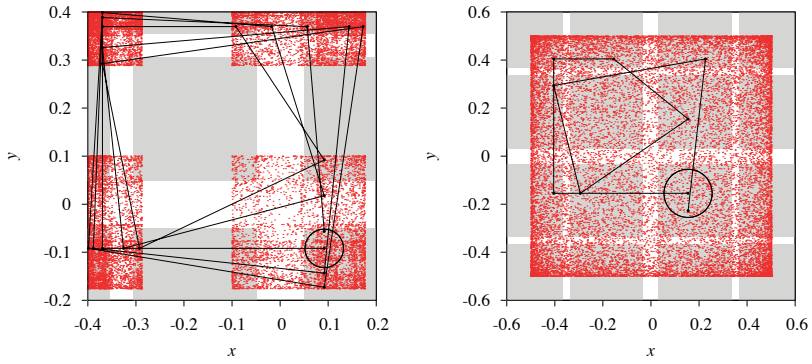

Figure 3.16. *Period-4 points as snapback repellers for $\mathscr{T}^4$ with $\varphi = \pi/2$. The grey areas indicate regions in which the eigenvalues of the matrix $D\mathscr{T}^4$ have an absolute value larger than 1. Line segments between iterates are added for clarity. In the left panel $a = 3.6$ and 20 iterations of $\mathscr{T}$ (i.e., 5 iterations of $\mathscr{T}^4$) are needed to end up in a fixed point of $\mathscr{T}^4$. In the right panel $a = 4$ and only 8 iterations (i.e., 2 iterations of $\mathscr{T}^4$) are needed.*

Appendix A.3. Then we checked whether such a preimage returns to an expanding neighborhood ball the fixed point. Note that the number of inverses grows exponentially fast, and for this reason this algorithm is only applicable to snap-back repellers with small "return times".

The period-p points that are born through the HNS bifurcation can also become snap-back repellers for the maps $\mathscr{P}^p$, $\mathscr{L}^p$, and $\mathscr{T}^p$ for suitable parameter values. We consider two different scenario's. In the first scenario a saddle periodic point forming a Hénon-like attractor becomes unstable through a period doubling bifurcation. As an example we consider the map $\mathscr{P}$ in the 1:5 resonance tongue. For $(a, b) = (3.85, 3.2)$ the Hénon-like attractor is shown in Figure 3.12. Numerical continuation shows that the saddle period-5 point becomes a source due to a period doubling bifurcation at $b \approx 3.404$. At $b = 3.6$ the period-5 points are expanding fixed points of the map $\mathscr{P}$, and in fact they are snap-back repellers. One such snap-back repeller is shown in Figure 3.20; the remaining four snap-back repellers are not shown.

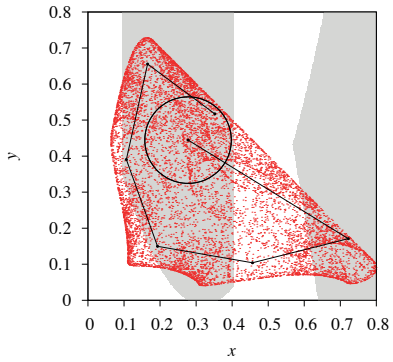

Figure 3.17. *A chaotic attractor of the predator-prey map $\mathscr{P}$ for $(a, b) = (3.6, 3.6)$. The regions for which the Jacobian matrix of $\mathscr{P}$ has two unstable eigenvalues are indicated in grey. The point $(0.277778, 0.444444)$ is an expanding fixed point which is in fact a snap-back repeller: an orbit of length 6 of preimages (indicated with dots and line segments to guide the eye) of this point enters a ball of radius $r = 0.12$ around the fixed point.*

Another scenario is the coexistence of a saddle periodic point leading to a Hénon-like attractor with a snap-back repeller. As an example we consider the 1:4 resonance tongue for the map $\mathscr{L}$. For $(\alpha, \tau) = (0.28, 2.25)$ the Hénon-like attractor is shown in Figure 3.13. Within the resonance tongue the saddle period-4 points coexists with a period-4 point which is a source. The numerical evidence of Figure 3.21 suggests that this point is a snap-back repeller for the map $\mathscr{L}^4$.

3.4.4 Loss of hyperbolicity

The Lyapunov diagrams of Figures 3.1–3.3 suggest that chaotic attractors with two positive Lyapunov exponents occur within sets of positive measure in the parameter plane of each of the maps $\mathscr{P}$, $\mathscr{L}$, and $\mathscr{T}$. It is an interesting question what bifurcation sequences lead to the formation of such attractors and what their geometric structure is. For the map $\mathscr{T}$ the latter question can be answered in the case $\varphi = \pi/2$ since then $\mathscr{T}^2$ is just given by decoupled

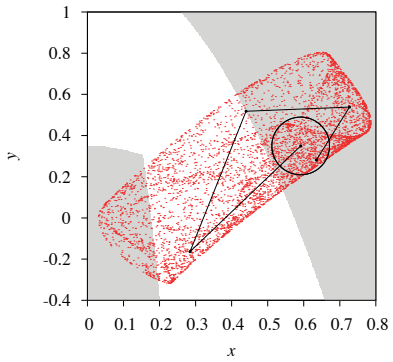

Figure 3.18. *As Figure 3.18, but for the map* $\mathscr{L}$ *with* $(\alpha, \tau) = (0.35, 2.1)$*, the fixed point* $(0.591608, 0.35)$*,* $m = 4$*, and* $r = 0.08$*.*

iterates of the logistic map in the x and y components. This implies that the attractor is simply the Cartesian product of two cantor sets.

The Lyapunov diagrams in Figures 3.9–3.11 suggest that the second Lyapunov exponent becomes positive in a continuous manner as a parameter is varied. This phenomenon might be related to loss of hyperbolicity. Abraham and Smale [1] constructed an example of a map for which dimension of the unstable subspace changes from point to point. The terminology *unstable dimension variability* was coined in [33]. In our maps the following scenario is possible. In a chaotic attractor the unstable periodic points are dense, and upon parameter variation more and more periodic points change from saddles to sources. We will not investigate this in the present work since this scenario is not specific to non-invertible maps, but for more details see [3, 4, 20, 22].

3.5 Discussion

In this Chapter we have studied the dynamics of three non-invertible, planar maps. These maps have as common properties that they rotate and fold the plane. It is clear that the maps are *not* related to each other by conjugation. Indeed, the map $\mathscr{L}$ cannot be conjugate to the maps $\mathscr{P}$ and $\mathscr{T}$ due to

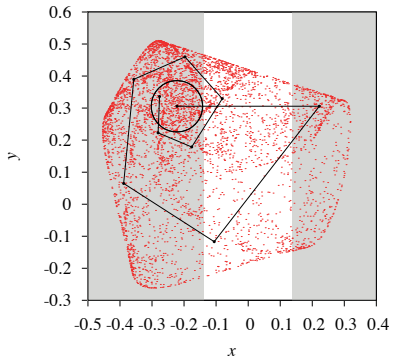

Figure 3.19. *As Figure 3.18, but for the map* $\mathscr{T}$ *with* $(a, \varphi_d) = (3.6, 72)$*, the fixed point* $(-0.222222, 0.305863)$*,* $m = 9$*, and* $r = 0.08$*.*

different number of pre-images. The maps $\mathscr{P}$ and $\mathscr{T}$ cannot be conjugate since otherwise the bifurcation sequences in their 1:5 resonance tongue would be the same.

Despite the lack of conjugacy the three maps share many similarities in both their dynamics and their bifurcations. We have analytically proven the existence of a Hopf–Neĭmark–Sacker bifurcation, which gives rise to resonance tongues in the parameter plane of the map. Inside a resonance tongue a periodic attractor typically either undergoes a period doubling cascade, which leads to chaotic dynamics, or a another Hopf–Neĭmark–Sacker bifurcation, which in turn leads to a new family of tongues. For all maps we have detected chaotic attractors of Hénon-like type: these attractors are conjectured to be the closure of an unstable manifold of a saddle periodic point. Due to the non-invertibility of the map these attractors have a folded structure which can be explained by means of the iterates of the critical line. In addition, we have detected snap-back repellers which may coexist with Hénon-like attractors.

We conjecture that the dynamics described above is typical for planar maps that rotate and fold the plane. We even conjecture that the map $\mathscr{T}$ may serve as a *prototype* for such maps. The advantage of the map $\mathscr{T}$ is that the action of folding and rotation can be controlled separately through the parameters a and φ. In particular, for $\varphi = \pi/2$ we were able to analytically

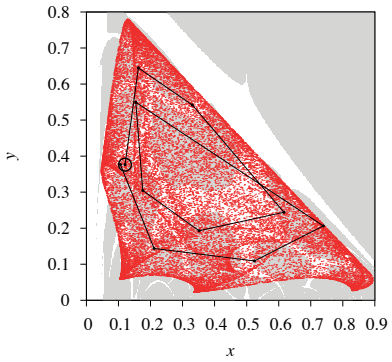

Figure 3.20. *A period-5 point for $\mathscr{P}$ acting as a snap-back repeller for $\mathscr{P}^5$ for $(a, b) = (3.85, 3.6)$. Note that there are 4 more period-5 points which are a snap-back repeller for $\mathscr{P}^5$, but these are not shown.*

prove the existence of snap-back repellers for the fourth iterate of $\mathscr{T}$. Note that our definition of $\mathscr{T}$ can also be used to consider more complicated non-invertible maps. For example, in (3.3) we can replace the function $f(x) = \frac{1}{4}(a-2) - ax^2$ by a function that has more than two preimages. A concrete example of such a map could be $f(x) = ax(x^2 - 1)$. Another choice for f would be the so-called tent map. In this case the fold-and-twist map $\mathscr{T}$ is not smooth, but it may be amenable to a more rigorous investigation. This approach is comparable to the Lozi map that was devised to get a better understanding of the Hénon map. We hope that our map $\mathscr{T}$ with various choices of the map f will inspire other researchers to obtain rigorous theorems for classes of planar, non-invertible maps.

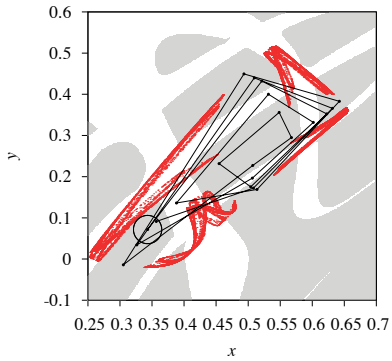

Figure 3.21. *A period-4 point of $\mathscr{L}$ acting as a snap-back repeller for $\mathscr{L}^4$ for $(\alpha, \tau) = (0.28, 2.25)$. Note that there are 3 more period-4 points which are a snap-back repeller for $\mathscr{T}^4$, but these are not shown. These snap-back repellers coexist the Hénon-like attractor for Figure 3.13.*

Appendix A

Technical details

A.1 Stability of periodic points

The stability of a period-p point of any differentiable map $\mathscr{F} : \mathbb{R}^2 \to \mathbb{R}^2$ can be easily determined from the so-called stability triangle [5]. Let T and D denote respectively the trace and the determinant of the Jacobian matrix of $\mathscr{F}^p$ evaluated at the period-p point. The eigenvalues of this matrix are then given by

$$\lambda_\pm = \frac{T \pm \sqrt{T^2 - 4D}}{2}.$$

The periodic point is stable when $|\lambda_\pm| < 1$, which is the case if and only if

$$-1 < D < 1 \quad \text{and} \quad -1 - D < T < 1 + D. \tag{A.1}$$

These inequalities determine a triangular region in the (T, D)-plane, see Figure A.1. The eigenvalues are real (resp. complex) for $D \leq T^2/4$ (resp. $D > T^2/4$). The periodic point loses stability by crossing the boundaries of the stability triangle in the following way:

- Crossing the line $D = 1$ implies that the complex pair $\lambda_\pm$ crosses the unit circle;
- Crossing the line $T = 1 + D$ implies that λ_+ passes through 1;
- Crossing the line $T = -1 - D$ implies that λ_- passes through -1.

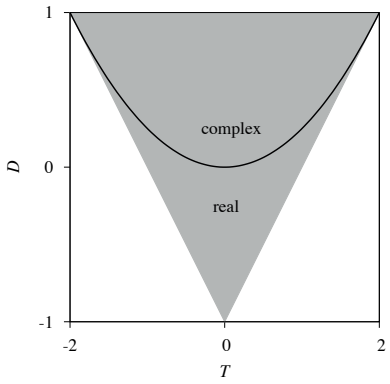

Figure A.1. *Let T and D respectively denote the trace and determinant of the Jacobian matrix of a map $\mathscr{F}$ evaluated at a periodic point. For values of (T, D) within the grey triangle the periodic point is stable. For $D > T^2/4$ the Floquet multipliers of the periodic point are complex.*

A.2 Normal form coefficients

Assume that a differentiable map $\mathscr{F} : \mathbb{R}^2 \to \mathbb{R}^2$ has a fixed point x_0 at which the Jacobian matrix J has two complex conjugate eigenvalues $e^{\pm i\theta}$ on the unit circle. This indicates that the fixed point x_0 bifurcates through a Hopf-Neĭmark-Sacker (HNS) bifurcation. Let $p, q \in \mathbb{C}^2$ be vectors satisfying the relations

$$Jq = \lambda q, \quad J^\top p = \bar{\lambda} p, \quad \langle p, q \rangle = 1, \tag{A.2}$$

where $\langle \cdot, \cdot \rangle$ denotes the standard innerproduct on $\mathbb{C}^2$ which is conjugate linear in the *first* component and linear in the *second* component. Define the function

$$H(z, \bar{z}) = \langle p, \mathscr{F}(x_0 + zq + \bar{z}\bar{q}) - x_0 \rangle$$

and consider its Taylor expansion around $(z, \bar{z}) = (0, 0)$:

$$H(z, \bar{z}) = e^{i\theta} z + \sum_{2 \le j+k \le 3} \frac{1}{j!k!} h_{jk} z^j \bar{z}^k + O(|z|^4).$$

The first Lyapunov coefficient is then defined by

$$\ell_1 = \mathrm{Re}\left(\frac{e^{-i\theta}h_{21}}{2} - \frac{(1-2e^{i\theta})e^{-2i\theta}}{2(1-e^{i\theta})}h_{20}h_{11}\right) - \frac{1}{2}|h_{11}|^2 - \frac{1}{4}|h_{02}|^2. \qquad \text{(A.3)}$$

Theorem 4.6 of [34] implies that if $\ell_1 < 0$ then the HNS bifurcation is supercritical, which means that a unique stable, closed invariant curve is born as the fixed point loses stability. Note that for maps with only quadratic nonlinear terms we always have that $h_{21} = 0$ which leads to a simplification of the expression for ℓ_1.

If J is a *real* 2×2 matrix, then the vectors $p, q \in \mathbb{C}^2$ satisfying equation (A.2) can be chosen as

$$q = \begin{pmatrix} a_{12} \\ e^{i\theta} - a_{11} \end{pmatrix}, \quad p = \frac{1}{a_{12}a_{21} + (e^{-i\theta} - a_{11})^2}\begin{pmatrix} a_{21} \\ e^{-i\theta} - a_{11} \end{pmatrix}, \qquad \text{(A.4)}$$

or, alternatively as

$$q = \begin{pmatrix} e^{i\theta} - a_{22} \\ a_{21} \end{pmatrix}, \quad p = \frac{1}{(e^{-i\theta} - a_{22})^2 + a_{12}a_{21}}\begin{pmatrix} e^{-i\theta} - a_{22} \\ a_{12} \end{pmatrix}. \qquad \text{(A.5)}$$

A.3 Preimages of the maps $\mathscr{P}$, $\mathscr{L}$, and $\mathscr{T}$

Preimages of the predator-prey map. Given a point $(u, v) \in \mathbb{R}^2$ we want to find all points (x, y) such that $(u, v) = \mathscr{P}(x, y)$, or equivalently,

$$\begin{aligned} u &= ax(1 - x - y), \\ v &= bxy. \end{aligned}$$

This gives

$$bu + av = abx(1 - x),$$

so that

$$x = \tfrac{1}{2} \pm \sqrt{\tfrac{1}{4} - \tfrac{u}{a} - \tfrac{v}{b}}.$$

After solving for x we find $y = v/bx$.

Preimages of the Lorenz map. Given a point $(u, v) \in \mathbb{R}^2$ we want to find all points (x, y) such that $(u, v) = \mathscr{L}(x, y)$, or equivalently,

$$\begin{aligned} u &= (1 + \alpha\tau)x - \tau xy, \\ v &= (1 - \tau)y + \tau x^2. \end{aligned}$$

From the second equation we obtain $y = (v - \tau x^2)/(1 - \tau)$. Substitution into the first equation then gives the cubic equation $x^3 + px + q = 0$, where

$$p = -\frac{1}{\tau}\left(v - \frac{(1-\tau)(1+\alpha\tau)}{\tau}\right), \quad q = -\frac{(1-\tau)u}{\tau^2},$$

provided that $\tau > 0$. If we know one solution of the cubic equation, say ξ, then a long division gives the quadratic equation $x^2 + \xi x + p + \xi^2 = 0$ by which we can find remaining solutions whenever $-3\xi^2 - 4p \geq 0$. In numerical computations of preimages the initial solution ξ can be found using the Newton-Raphson method.

Preimages of the fold-and-twist map. Given a point $(u, v) \in \mathbb{R}^2$ we want to find all points (x, y) such that $(u, v) = \mathscr{T}(x, y)$, or equivalently,

$$\begin{aligned} u &= f(x)\cos\varphi - y\sin\varphi, \\ v &= f(x)\sin\varphi + y\cos\varphi. \end{aligned}$$

This gives

$$u\cos\varphi + v\sin\varphi = f(x) = \tfrac{1}{4}(a-2) - ax^2,$$

so that

$$x = \pm\sqrt{\frac{a - 2 - 4u\cos\varphi - 4v\sin\varphi}{4a}}.$$

Finally,

$$y = v\cos\varphi - u\sin\varphi.$$

Appendix B

Numerical methods

In this Section we briefly describe the numerical algorithms that we have used to compute Lyapunov exponents and unstable manifolds of saddle points. The algorithms apply to any general smooth map $\mathscr{F} : \mathbb{R}^d \to \mathbb{R}^d$.

B.1 Computation of Lyapunov exponents

We estimate Lyapunov exponents using the algorithm described in [9, 10]. Given an initial condition we first iterate the map N_{trans} times to obtain a point x_1 on the attractor. Let $u_{1,k}$ denote the k-th standard basis vector of $\mathbb{R}^d$. At each point x_n on the orbit we apply the Jacobian matrix $D\mathscr{F}(x_n)$ to each of the vectors $u_{n,k}$. Each vector tends to align itself along the direction of maximal expansion (or of minimal compression). To prevent the vectors $u_{n,k}$ from collapsing onto one direction the Gram-Schmidt process is used. The average of the logarithms of the rescaling factors then gives an approximation of the k-th Lyapunov exponent.

Let $\langle \cdot, \cdot \rangle$ denote the standard inner product on $\mathbb{R}^d$. For $n \geq 1$ we have

applied the following iteration scheme:

$$\begin{aligned} v_{n,k} &= D\mathscr{F}(x_n)u_{n,k}, \\ u_{n,1} &= v_{n,1}, \\ u_{n,k} &= v_{n,k} - \sum_{j=1}^{k-1} \frac{\langle v_{n,k}, u_{n,j}\rangle}{\langle u_{n,j}, u_{n,j}\rangle} u_{n,j}, \\ u_{n+1,k} &= u_{n,k}/\|u_{n,k}\|, \\ x_{n+1} &= \mathscr{F}(x_n). \end{aligned}$$

Iterating this scheme N times then gives the following approximation for the k-th Lyapunov exponent:

$$\lambda_k = \frac{1}{N}\sum_{n=1}^{N} \log \|u_{n,k}\|.$$

Typical values used in our computations are $N_{trans} = 10^3$ and $N = 10^4$.

B.2 Computation of power spectra

By evaluating a scalar observable $\omega : \mathbb{R}^d \to \mathbb{R}$ along an orbit of the map F we produce a scalar time series of length N. First, we subtract the mean of the time series. Next, a Hamming window is applied to reduce leakage of frequencies: we multiply the k-th element of the time series by the number

$$H_k = 0.54 - 0.46\cos\left(\frac{2\pi k}{N}\right), \qquad k = 0, \ldots, N-1.$$

Finally, we normalize the time series by dividing each element by the norm of the array $(H_k)_{k=0}^{N-1}$. Denote the resulting time series by $(c_k)_{k=0}^{N-1}$. From this time we compute a discrete Fourier transform (DFT) by

$$\widehat{c}_k = \frac{1}{N}\sum_{n=0}^{N-1} c_n \exp\left(-2\pi i \frac{nk}{N}\right). \tag{B.1}$$

The power spectrum is a plot of $|\widehat{c}_k|^2$ against the Fourier frequency $f_k = k/N$. All frequencies are computed modulo 1, and since our time series is real-valued its DFT is symmetric around the frequency $f = 1/2$. Indeed, from (B.1) it follows that $\widehat{c}_{N-k} = \widehat{c}_k^*$.

For the fold-and-twistmap (3.3) we have used the observable $\omega(x, y) = x$ and computed the DFT (B.1) by means of a fast Fourier transform implemented in the FFTW library [23].

B.3 Computation of unstable manifolds

We compute unstable manifolds of periodic points by means of techniques based on iterating fundamental domains described in [18, 51]. Note that for non-invertible maps the unstable manifold can have self-intersections. Hence the terminology "manifold" is strictly speaking not correct.

Let x be a fixed point of the map $\mathscr{F}$. Assume that the Jacobian matrix $D\mathscr{F}(x)$ has one real eigenvalue $\lambda > 1$ with corresponding eigenvector v and all the other eigenvalues have absolute value strictly smaller than 1. If we want to approximate N points on the manifold, we first compute a linear approximation of the manifold in a small neighborhood of the point x:

$$\begin{aligned} s_j &= \varepsilon \exp(j \log(\lambda^2)/N), \\ w^L_{0,j} &= x - s_j v, \\ w^R_{0,j} &= x + s_j v, \end{aligned}$$

where $j = 1, \ldots, N$. The superscripts L and R indicate the "left" and "right" branch of the manifold, respectively. Then, for $1 \le k \le m$ we define inductively

$$\begin{aligned} w^L_{k,j} &= \mathscr{F}(w^L_{k-1,j}), \\ w^R_{k,j} &= \mathscr{F}(w^R_{k-1,j}). \end{aligned}$$

The "left" branch of the unstable manifold is then approximated by connecting the points

$$w_{0,1}, \ldots, w_{0,N}, w_{1,1}, \ldots, w_{1,N}, \ldots, w_{m,1}, \ldots, w_{m,N}$$

by line segments. The "right" branch is computed in the same way. For a periodic point x with period p we apply the above procedure with $\mathscr{F}$ replaced by $\mathscr{F}^p$ to each of the points $x, \mathscr{F}(x), \ldots, \mathscr{F}^{p-1}(x)$ along the periodic orbit. Table B.1 lists the parameters ε, N, and m that were used to produce our figures.

Figure no.	ε	N	m
3.6	0.001	10	25
3.12	0.0001	1000	8
3.13	0.0001	1000	9
3.14	0.0001	1000	9

Table B.1. *Parameters used in the computation of unstable manifolds.*

Bibliography

[1] R. Abraham and S. Smale. *Nongenericity of Ω-stability*, volume 14 of *Global Analysis, Symp. Pure Math.* American Mathematical Society, 1970.

[2] V.S. Afraimovich, V.V. Bykov, and L.P. Shil'nikov. Origin and structure of the Lorenz attractor. *Akademiia Nauk SSSR Doklady*, 234:336–339, 1977.

[3] K.T. Alligood and E. Sander. Crossing bifurcations and unstable dimension variability. *Physical Review Letters*, 96:244103, 2006.

[4] D. Auerbach, P. Cvitanović, J.-P. Eckmann, G. Gunaratne, and I. Procaccia. Exploring chaotic motion through periodic orbits. *Physical Review Letters*, 58:2387–2389, 1987.

[5] E. Barreto, B.R. Hunt, C. Grebogi, and J.A. Yorke. From high dimensional chaos to stable periodic orbits: the structure of parameter space. *Physical Review Letters*, 78:4561, 1997.

[6] J.R. Beddington, C.A. Free, and J.H. Lawton. Dynamic complexity in predator-prey models framed as difference equations. *Nature*, 255:58–60, 1976.

[7] M. Benedicks and L. Carleson. On iterations of $1 - ax^2$ on $(-1, 1)$. *Annals of Mathematics*, 122:1–25, 1985.

[8] M. Benedicks and L. Carleson. The dynamics of the Hénon map. *Annals of Mathematics*, 133:73–169, 1991.

[9] G. Benettin, L. Galgani, A. Giorgilli, and J.-M. Strelcyn. Lyapunov characteristic exponents for smooth dynamical systems and for Hamiltonian systems; a method for computing all of them. Part 1: theory. *Meccanica*, 15:9–20, 1980.

[10] G. Benettin, L. Galgani, A. Giorgilli, and J.-M. Strelcyn. Lyapunov characteristic exponents for smooth dynamical systems and for Hamiltonian systems; a method for computing all of them. Part 2: numerical application. *Meccanica*, 15:21–30, 1980.

[11] H.W. Broer, R. Roussarie, and C. Simó. On the Bogdanov-Takens bifurcation for planar diffeomorphisms. In C. Perelló, C. Simó, and J. Solà-Morales, editors, *Equadiff 1991, Proceedings Western European Conference on Differential Equations, Barcelona 1991*, pages 81–92. World Scientific, 1993.

[12] H.W. Broer, C. Simó, and J.C. Tatjer. Towards global models near homoclinic tangencies of dissipative diffeomorphisms. *Nonlinearity*, 11:667–770, 1998.

[13] H.W. Broer, C. Simó, and R. Vitolo. Bifurcations and strange attractors in the Lorenz-84 climate model with seasonal forcing. *Nonlinearity*, 15:1205–1267, 2002.

[14] H.W. Broer, C. Simó, and R. Vitolo. Quasi-periodic hénon-like attractors in the Lorenz-84 climate model with seasonal forcing. In F. Dumortier, H.W. Broer, J. Mahwin, A. Vanderbauwhede, and S.M. Verduyn-Lunel, editors, *Equadiff 2003, Proceedings International Conference on Differential Equations, Hasselt 2003*, pages 714–719. World Scientific, 2005.

[15] H.W. Broer, C. Simó, and R. Vitolo. Hopf saddle-node bifurcation for fixed points of 3d-diffeomorphisms: Analysis of a resonance 'bubble'. *Physica D*, 237:1773–1799, 2008.

[16] H.W. Broer, C. Simó, and R. Vitolo. The Hopf-saddle-node bifurcation for fixed points of 3D-diffeomorphisms: the Arnol′d resonance web. *Bulletin of the Belgian Mathematical Society Simon Stevin*, 15:769–787, 2008.

[17] H.W. Broer, C. Simó, and R. Vitolo. Chaos and quasi-periodicity in diffeomorphisms of the solid torus. *Discrete and Continuous Dynamical Systems B*, 14:871–905, 2010.

[18] H.W. Broer and F. Takens. *Dynamical Systems and Chaos*, volume 172 of *Applied Mathematical Sciences*. Springer, 2010.

[19] X. Chen, S. Yuan, Z. Jing, and X. Fu. Bifurcation and chaos of a discrete-time mathematical model for tissue inflammation. *Journal of Dynamics and Difference Equations*, 28:281–299, 2016.

[20] R. Davidchack and Y.-C. Lay. Characterization of transition to chaos with multiple positive Lyapunov exponents by unstable periodic orbits. *Physics Letters A*, 270:308–313, 2000.

[21] L. Díaz, J. Rocha, and M. Viana. Strange attractors in saddle cycles: Prevalence and globality. *Inventiones Mathematicae*, 125:37–74, 1996.

[22] V. Dos Santos, J.D. Szezech Jr., M.S. Baptista, A.M. Batista, and I.L. Caldas. Unstable dimension variability structure in the parameter space of coupled Hénon maps. *Applied Mathematics and Computation*, 286:23–28, 2016.

[23] Matteo Frigo and Steven G. Johnson. The design and implementation of FFTW3. *Proceedings of the IEEE*, 93(2):216–231, 2005.

[24] L. Gardini and F. Tramontana. Snap-back repellers and chaotic attractors. *Physical Review E*, 81:046202, 2010.

[25] L. Gardini and F. Tramontana. Snap-back repellers in non-smooth functions. *Regular and Chaotic Dynamics*, 15:237–245, 2010.

[26] S. Garst and A.E. Sterk. The dynamics of a fold-and-twist map. *Indagationes Mathematicae*, 27:1279–1304, 2016.

[27] S. Garst and A.E. Sterk. Periodicity and chaos amidst twisting and folding in 2-dimensional maps. Accepted for publication in *International Journal of Bifurcation and Chaos*, 2018.

[28] J. Guckenheimer and P. Holmes. *Nonlinear oscillations, dynamical systems and bifurcations of vector fields*, volume 42 of *Applied Mathematical Sciences*. Springer, 1983.

[29] J. Guckenheimer and R.F. Williams. Structural stability of Lorenz attractors. *Publications Mathématiques de l'Institut des Hautes Études Scientifiques*, 50:59–72, 1979.

[30] I. Gumowski and C. Mira. Sur un algorithme de détermination du domaine de stabilité d'un point d'une récurrence non linéaire du deuxième ordre à variables réelles. *Comptes Rendus Acad. Sc. Paris, Série A*, 260:6524–6527, 1965.

[31] I. Gumowski and C. Mira. Sensitivity problems related to certain bifurcations in nonlinear recurrences relations. *Automatica*, 5:303–317, 1969.

[32] M. Hénon. A two dimensional mapping with a strange attractor. *Communications in Mathematical Physics*, 50:69–77, 1976.

[33] E.J. Kostelich, I. Kan, C. Grebogi, E. Ott, and J.A. Yorke. Unstable dimension variability: a source of nonhyperbolicity in chaotic systems. *Physica D*, 109:81–90, 1997.

[34] Yu.A. Kuznetsov. *Elements of Applied Bifurcation Theory*, volume 112 of *Applied Mathematical Sciences*. Springer, third edition, 2004.

[35] M.-C. Li and M.-J. Lyu. A simple proof for persistence of snap-back repellers. *Journal of Mathematical Analysis and Applications*, 352:669–671, 2009.

[36] T.-Y. Li and J.A. Yorke. Period three implies chaos. *The American Mathematical Monthly*, 82:985–992, 1975.

[37] E.N. Lorenz. Deterministic nonperiodic flow. *Journal of the Atmospheric Sciences*, 20:130–141, 1963.

[38] E.N. Lorenz. Computational chaos – a prelude to computational instability. *Physica D*, 35:299–317, 1989.

[39] F.R. Marotto. Snap-back repellers imply chaos in $\mathbb{R}^n$. *Journal of Mathematical Analysis and Applications*, 63:199–223, 1978.

[40] F.R. Marotto. Chaotic behavior in the Hénon mapping. *Communications in Mathematical Physics*, 68:187–194, 1979.

[41] F.R. Marotto. On redefining a snap-back repeller. *Chaos, Solitons and Fractals*, 25:25–28, 2005.

[42] C. Mira. Détermination practique du domaine de stabilité d'un point d'équilibre d'une récurrence non linéaire du deuxième ordre à variables réelles. *Comptes Rendus Acad. Sc. Paris, Série A*, 261:5314–5317, 1964.

[43] C. Mira, D. Fournier-Prunaret, Gardini L., H. Kawakami, and J.C. Cathala. Basin bifurcations of two-dimensional non-invertible maps: fractalization of basins. *International Journal of Bifurcations and Chaos*, 4:343–381, 1994.

[44] C. Mira, L. Gardini, A. Barugola, and J.C. Cathala. *Chaotic Dynamics in Two-Dimensional Noninvertible Maps*. World Scientific Publishing, 1996.

[45] L. Mora and M. Viana. Abundance of strange attractors. *Acta Mathematicae*, 171:1–71, 1993.

[46] J. Palis and F. Takens. *Hyperbolicity and sensitive chaotic dynamics at homoclinic bifurcations*. Cambridge University Press, 1993.

[47] C.-C. Peng. Numerical computations of orbits and rigorous verification of existence of snapback repellers. *Chaos*, 17:013107, 2007.

[48] J. Ren, L. Yu, and S. Siegmund. Bifurcations and chaos in a discrete predator-prey model with Crowley-Martin functional response. *Nonlinear Dynamics*, 90:19–41, 2017.

[49] S.M. Salman, A.M. Yousef, and A.A. Elsadany. Stability, bifurcation analysis and chaos control of a discrete predator-prey system with square root functional response. *Chaos, Solitons and Fractals*, 93:20–31, 2016.

[50] Y. Shi and P. Yu. Chaos induced by regular snap-back repellers. *Journal of Mathematical Analysis and Applications*, 337:1480–1494, 2008.

[51] C. Simó. On the analytical and numerical continuation of invariant manifolds. In D. Benest and C. Froeschlé, editors, *Modern Methods in Celestial Mechanics*, pages 285–330. Éditions Frontières, 1990.

[52] S. Smale. Differentiable dynamical systems. *Bulletin of the American Mathematical Society*, 73:747–817, 1967.

[53] S. Smale. Finding a horseshoe on the beaches of Rio. *The Mathematical Intelligencer*, 20:39–44, 1998.

[54] M. Viana. Strange attractors in higher dimensions. *Bulletin of the Brazilian Mathematical Society*, 24:13–62, 1993.

[55] M. Viana. What's new on Lorenz strange attractors? *The Mathematical Intelligencer*, 22(3):6–19, 2000.

[56] R. Vitolo, H.W. Broer, and C. Simó. Routes to chaos in the Hopf-saddle-node bifurcation for fixed points of 3D-diffeomorphisms. *Nonlinearity*, 23:1919–1947, 2010.

[57] R.F. Williams. The structure of the Lorenz attractor. *Publications Mathématiques de l'Institut des Hautes Études Scientifiques*, 50:72–99, 1979.

[58] Wolfram Research, Inc. Mathematica, Version 11.0.1.0, 2016. Champaign, IL, 2016.

[59] S. Yuan, T. Jiang, and Z. Jing. Bifurcations and chaos in the Tinkerbell map. *International Journal of Bifurcations and Chaos*, 21:3137–3156, 2011.

[60] M. Zhao and C. Li. Complex dynamic behaviour of an economic cycle model. *Journal of Difference Equations and Applications*, 22:1777–1790, 2016.

Samenvatting

De aanleiding

De oorsprong van dit proefschrift ligt in de jaren tachtig als H. Lauwerier op het Mathematisch Congres in Delft het dynamisch gedrag van onder andere een prooi-roofdier model bespreekt. Zijn plaatjes tonen verrassende structuren die met een eenvoudige computer te maken zijn. Een eerste analyse van de prooi-roofdier afbeelding was al beschreven in [2] waarbij het werk van Mira [3] een waardevolle aanvulling is. In Mira's werk wordt de rol van kritieke krommen die voorkomen in de prooi-roofdier afbeelding uitbundig beschreven.

Eerste analyse

Na een inventarisatie van de eigenschappen van de prooi-roofdier afbeelding, zoals welke gebieden worden op welke andere gebieden afgebeeld, wordt de dynamica die de herhaalde toepassing van de afbeelding genereert het onderwerp van studie. In één van de dekpunten heeft de afgeleide (de Jacobiaan) complexe eigenwaarden en voor geschikt gekozen waarden van de parameters is de norm van die eigenwaarden groter dan één. Binnen het invariante gebied van de afbeelding zijn er punten waarbij de determinant van de Jacobiaan gelijk is aan nul. Het beeld van deze punten vormen de kritieke lijn die samen met de eerst volgende iteraties de rand van een invariant gebied vormen. De kritieke lijn en de complexe eigenwaarden in een van de fixpunten zijn de inspiratie voor de definitie van de vouw en draai afbeelding, de Fold and Twist.

Fold and Twist

Voor de definitie van de Fold and Twist beschouwen we de verzameling van verticale lijnen $x = c$ in het vlak. We passen op die lijnen een met de logistische afbeelding geconjungeerde afbeelding $f(x) = \frac{1}{4}(a-2) - ax^2$ toe en laten daarbij de y-coördinaten van de punten op die lijnen onveranderd. Op de nu ontstane verzameling verticale lijnen wordt een rotatie om de oorsprong over een hoek φ uitgevoerd.
De Fold and Twist heeft twee dekpunten waarvan er de ene op de rand en de andere in het binnengebied ligt van de verzameling van punten die niet naar oneindig convergeren.
Omdat bij de prooi-roofdier afbeelding periode zes prominent voorkomt gaat bij de Fold-and-Twist allereerst de aandacht uit naar een baan van die periode. Periodieke punten kunnen gevonden worden via de snijpunten van twee krommen. Zie [1]. Er zijn dan *twee* banen van periode zes. De zadelpunten van een van de twee banen liggen op de gemeenschappelijke rand van de basins van de aantrekkende punten van de andere baan van periode zes. Zo kan een saddle-node bifurcatie ontstaan voor een geschikt gekozen waarde van de parameters. De Fold and Twist afbeelding is zodanig gedefineerd dat verschillende analytische resultaten te boeken zijn. Zo kan het voorkomen van een *Hopf-Neĭmark-Sacker* bifurcatie worden bewezen voor rotaties over alle hoeken met uitzondering van $\varphi = 90°$ en $\varphi = 120°$. Voor $\varphi = 90°$ en $\varphi = 120°$ kunnen de banen van periode vier respectievelijk periode drie exact worden berekend.

De drie afbeeldingen

De vouw en draai eigenschap voor de Fold and Twist afbeelding zijn ook gevonden bij de eerder genoemde prooi-roofdier afbeelding en bij de discrete Lorenz-63 afbeelding. Dat maakt de Fold and Twist afbeelding tot een geschikt toy model voor twee dimensionale afbeeldingen met een vouw en een draai. Zo kunnen eenvoudig gevonden eigenschappen van de Fold and Twist afbeelding gezocht en gevonden worden bij de andere twee afbeeldingen.

Van lokaal naar globaal

Lyapunov exponenten geven aan van welk type dynamica er voor de gekozen waarde van de parameters sprake is. In het Lyapunov diagram worden voor de verschillende parameterwaarden de gevonden typen dynamica weergegeven. Vergelijken we de Lyapunov diagrammen van de Fold and Twist, de prooi-roofdier afbeelding en de discrete Lorenz-63 afbeelding dan valt de grote gelijkenis op tussen deze drie afbeeldingen. Deze gelijkenis voedt de claim dat de Fold and Twist fundamenteel is voor 2-d afbeeldingen met een kritieke lijn. Een deelverzameling van het Lyapunov diagram is die van de resonantie- of Arnold tongen. Binnen zo'n resonantietong bevinden zich de pararmeterwaarden waarvoor de afbeelding steeds een periodieke baan heeft kenmerkend voor die resonantietong. Op de rand van zo'n resonantietong treedt een saddle-node bifurcatie op. Binnen de resonantietongen is sprake van een cascade van periodeverdubbelingen of een secundaire *Hopf-Neĭmark-Sacker* bifurcatie.

Het chaotisch gedrag

Het Lyapunov diagram geeft aan dat er parameterwaarden zijn waarbij de afbeelding zich chaotisch gedraagt. Het bestaan van snap-back repellers wordt voor alle drie de afbeeldingen bewezen zodat via de stelling van Marotto het chaotisch gedrag vast staat.
Een andere vorm van chaotisch gedrag is die waarbij de attractor eigenschappen van de Hénon achtige attractor heeft. Zo zijn in de drie de afbeeldingen parameterwaarden gevonden worden waarbij de onstabiele variëteit van een onstabiel periodiek punt grote gelijkenis vertoont met de attractor.

Tot slot

Een dynamisch model in 2-D inspireerde tot de definitie van een toymodel waarvan de eigenschappen steeds in twee voorbeelden van 2-1 afbeeldingen voorkomen. Nadere studie moet uitwijzen of de Fold and Twist afbeelding fundamenteel is binnen de verzameling van de 2-1 afbeeldingen. Een eerste verkenning van een afbeelding met meer dan één vouw lijkt zich te gedragen als een Fold and Twist op de plaatsen van de vouwen. De constructie van een goed werkend toy model voor afbeeldingen in 3-D staat hoog op een verlanglijstje.

Bibliografie

[1] Davies, B., *Exploring Chaos*, Westview Press 2004.

[2] Lauwerier H., *Two-dimensional iterative maps*, in Chaos, ed. A.V. Holden, Manchester University Press 1986, pp 58-95

[3] Mira C.,Gardini L.,Barigola A. & Cathala J-C, *Chotic Dynamics in Two Dimensional Noninvertible Maps* in World Scientific Publishing(Singapore)

Acknowledgements

It was after a period of three years of LIO (Teachers in Research) in Delft that Jan Aarts suggested to continue the work we had done so far and to complete it with a dissertation. At that moment, Jan and I had analysed a predator-prey map after which we came to the conclusion that a study of the Fold and Twist map could be useful as a tool in understanding the dynamics of the predator-prey map. At first I was surprised by Jans proposal. However, my experience with the LIO-project had taught me that doing research inspired me in my daily work as a maths teacher.

Over a period of many years, Jan was already retired, I could work in the field of discrete dynamics. Jan, always present on Tuesdays, carried out his own research and published several books. Meanwhile, he inquired after my progress followed by some valuable suggestions. His patience was remarkable and a great example for me as a teacher. I am very grateful for his guidance and encouragement. We both looked forward to the defence of this dissertation. Unfortunately, life took a different turn.

Many people contributed to the completion of this work. First of all, Alef Sterk. I am grateful for all his suggestions and his experience in the preparation of the two articles we have published. Due to his computer machinery the figures in this dissertation could rise to a higher level.

I also wish to express my sincere thanks to Henk Broer, my promotor and supervisor. When the process was in danger of going in the wrong direction, it was Henk who came up with suggestions for the right one. For me it is

an honour that my defence is exactly 39 years after Henks defence of his dissertation.

I would like to acknowledge George Huitema for his suggestions in the final stage of this dissertation. His suggestions for a clear structure in the first chapter are very much appreciated.

Furthermore, I would like to thank my colleagues at RGO Middelharnis for their support during the many years I worked on this dissertation. Especially Peter Huysse and Jacqie Hoogervorst who were able to block the Tuesdays in my timetable for all those years.

These acknowledgements would not be complete without mentioning the mathematicians in Delft who encouraged me to continue my work on the Fold and Twist map. Thank you!

Finally, Swier (jr) and Jacqueline deserve my gratitude. I am thankful for their patience and support since their father/husband preferred doing maths to playing games.

Aantekeningen

Aantekeningen